Summer 8-31-2023

Nanodiscs: A novel approach to the study of the Methionine ABC Transporter System

Michael T. Winslow
University of San Francisco, mtwinslow1@gmail.com

Nanodiscs:

A novel approach to the study of the Methionine ABC Transporter System

A thesis presented to the faculty

of the Department of Chemistry

at the University of San Francisco

in partial fulfillment of the requirements for the degree of

Master of Science in Chemistry

Written by

Michael Winslow

Bachelor of Science in Biochemistry and Molecular Biology

University of California, Santa Cruz

August 2023

Nanodiscs:

A novel approach to the study of the Methionine ABC Transporter System

Thesis written by Michael Winslow

This thesis is written under the guidance of the Faculty Advisory Committee, and approved by all its members, has been accepted in partial fulfillment of the requirements for the degree of

Master of Science in Chemistry

at the University of San Francisco

Thesis Committee

Janet G. Yang, Ph.D.

Research Advisor

Jennifer Tripp, Ph. D.

Assistant Professor of Chemistry

Tami Spector, Ph.D.

Professor of Chemistry

Jeffrey Paris, Ph.D.

Acting Dean, College of Arts and Sciences

Acknowledgements

The list of individuals who have helped me to complete this work is vast, and I am truly grateful for all the contributions and support I have received to get where I am. First, and most importantly, I must express the gratitude I have for my research advisor, Janet Yang. Time and again Janet continues to fight tirelessly for her student's educations and opportunities, and guides them through their scientific endeavors. I can thank Janet for teaching me how to independently troubleshoot research projects, one of my most valuable skills which I continue to use in my career every day. Without Janet's dedication, this work would never have come to fruition, and she has continued to support me despite my challenges. Next, I must express my thanks for the various USF Faculty, my committee members, as well as students who helped me throughout my time here. I received help from multiple research assistants, namely Gabby Servito, Justin Winslow, and Daniel Borraez who likely taught me more about teaching and mentoring in a lab than I taught them. I would like to thank Dennis Hicks for being a sound and dedicated research peer, as well as other friends I made in the Chemistry and Biology Departments during our studies. I benefited greatly from the Whitehead Summer Research Fellowship, the extremely generous contributions from Jim and Lia Whitehead supported this project. I would also like to thank Jeff Oda and Deidre Shymanski, the former who helped us to set up a new lab and the latter who has kept me and countless students on track for success.

I received extraordinary help outside of USF as well. Frank Duong and his lab graciously hosted me in University of British Columbia for hands-on training as detailed in this work, and his students Katherine, Michael and John continued to offer advice after my visit. I also received expert advice working with specific proteins from Phong Nguyen and Jefferey Lai of Rees Lab at Cal Tech, that helped with purification. I received help from Dr. Narlikar and Dr. Shoichet of UCSF utilizing their instruments, and since have become a more advanced user of the Light Scattering techniques I initially attempted in this project. Lastly, I must acknowledge my family, who have also always been there to help me pursue my dreams and help during difficult times. I want to thank my parents, especially my father, "Dr. Winslow," for fostering my scientific curiosity, education and career, and my mother for keeping me committed even when challenged. I also want to thank both of my brothers Jonathan and Justin; the latter got the opportunity to work with me in the lab briefly. It was an absolute honor to begin in the Yang Lab, and look forward to seeing it grow. Thank you

Table of Contents

List of Figures

List of Tables

List of Abbreviations

ABC: ATP Binding Cassette
Abs_{280}: Absorption at 280 nm Wavelength Light
Alc-D: Alcohol Dehydrogenase
ATP: Adenosine Triphosphate
ADP: Adenosine Diphosphate
AU: Absorption Units
BN-PAGE: Blue Native Polyacrylamide Gel Electrophoresis
BME: β-mercaptoethanol
BSA: Bovine Serum Albumin
Co-IP: Co-Immunoprecipitation
CN-PAGE: Clear Native Polyacrylamide Gel Electrophoresis
CF: Correction Factor
CRD: C-terminal Regulatory Domain
DDM: n-Dodecyl β-D-maltoside
DNA: Deoxyribonucleic acid
DTT: Dithiothreitol
ECF: Energy Coupling Factor
EDTA: Ethylenediaminetetraacetic Acid
FPLC: Fast Protein Liquid Chromatography
IPTG: Isopropyl β- d-1-thiogalactopyranoside
K_{av}: Partition Coefficient
k_{cat}: Catalytic Constant or Turnover Number
kD: Kilodalton
K_D: Dissociation Constant
K_M: Michaelis Constant
kHz: Kilohertz
K_I: Inhibition Constant

LB: Luria Broth

n: Hill Coefficient

N/A: Not Applicable

NBD: Nucleotide Binding Domain

ND: Nanodisc consisting of Membrane Scaffold Proteins

Ni-NTA: Nickel-Nitrilotriacetic acid

M_r: Relative Molecular Mass

M_w: Molecular Weight

MESG: 2-amino-6-mercapto-7-methylpurine riboside

MetNI-ND1: Complex consisting of MetNI embedded in MSP1 Nanodisc

MetNI-ND3: Complex consisting of MetNI embedded in MSP3 Nanodisc

MetNIQ: E. coli Methionine ABC Transporter-Substrate Binding Protein Complex

MSP1: Membrane Scaffold protein MSP1D1

MSP3: Membrane Scaffold protein MSP1E3D1

OD 600: Optical Density at 600 nm Wavelength Light

SDS-PAGE: Sodium Dodecyl Sulfate Polyacrylamide Gel Electrophoresis

SBP: Substrate Binding Protein

SEC: Size Exclusion Chromatography

TAPS: [Tris(hydroxymethyl)methylamino]propanesulfonic Acid

TCEP: Tris(2-carboxyethyl)phosphine

TMD: Transmembrane Domain

TSG10: Tris-Buffered Saline containing 10% Glycerol

V_{max}: Maximum Velocity of an Enzymatic Reaction

Abstract

Membrane transporter proteins play the vital role of moving compounds in and out of the cell and are essential for all living organisms. ATP Binding Cassette (ABC) family transporters function both as importers and exporters in prokaryotes. MetNI is an *E. coli* Type I ABC transporter responsible for the uptake of methionine into the cytosol from the cell periplasmic space through the cell membrane to maintain intracellular methionine pools. ABC transporters, like other membrane proteins, are most often mechanistically and structurally studied *in vitro,* solubilized by detergents. However, detergent micelles may affect the conformational changes of membrane proteins relative to those in a native membrane lipid environment, altering transport and ATPase hydrolysis activities. The goal of this research project was to test a promising alternative to liposomal reconstitution of MetNI for preserving native activities. This system, termed "nanodiscs," is a well-established biochemical tool for membrane proteins consisting of a nanoscale discoidal bilayer of polar lipids encircled by an amphipathic scaffold of apolipoprotein ApoA1 proteins. In this work, the MetNI transporter was purified and successfully reconstituted into two different MSP phospholipid bilayer nanodisc systems (MSP1D1 and MSP1E3D1), confirmed by size exclusion chromatography, native gel electrophoresis, and co-immunoprecipitation. Stabilization of a more native MetNI structure following nanodisc reconstitution was evaluated by the level of basal ATP hydrolysis when compared with purified MetNI solubilized by detergent. Surprisingly, the K_M and V_{max} of ATP hydrolysis were similar for both forms of MetNI, indicating the presence of basal, futile ATP hydrolysis in both types. Futile ATP hydrolysis was also observed for a mutant MetNI form which lacks methionine substrate inhibition of ATP hydrolysis, MetNI N295A. Additionally, binding of purified substrate binding protein (SBP) to the detergent-solubilized and nanodisc-reconstituted MetNI transporter, was demonstrated by fluorescence anisotropy. Future functional assays performed on completely reconstituted MetNI-SBP complexes in lipid nanodiscs could reveal critical insights into the lipid and structural requirements for native transporter activity.

Chapter 1. Introduction to ABC Transporters and Nanodiscs

1.1 Membrane Proteins in Cellular Transport

Membrane transporter proteins play the vital role of moving compounds in and out of the cell and are essential for all living organisms. These integral membrane proteins provide a structural opening for compounds, ranging from atomic ions to macromolecules, so that they may overcome the physical boundary of hydrophobic plasma and organelle membranes. Without these transport proteins, cells would not be able to acquire nutrients or prevent waste, toxins or products from accumulating within. Due to the wide variety of compounds translocated, protein transporters have become highly specialized for specific compounds, or whole classes of molecules, over the course of evolution. Some membrane transport proteins known as “carriers” simply offer a channel for molecules to diffuse through the membrane or facilitate diffusion in one direction to restrict reverse flow (passive transport), while others utilize the chemical energy stored in adenosine triphosphate (ATP) or electrochemical gradients to “pump” the compounds against a concentration gradient (active transport). The cost of pumping molecules across the membrane is theorized to be approximately 10-60% of the cell’s energy expenditure in bacteria and in humans [1-3]. Understanding how these transporters are structured, function, and regulated to drive cellular processes, export products, and ultimately achieve homeostasis by balancing intracellular concentrations, is an imperative field of biochemical research and structural biology. Although many different transporters have been characterized structurally and functionally, their complex structures and sensitive dispositions have made them challenging to study, and much about them remains unknown. However, advances in technology and new discoveries have led to different theories, particularly in the transporter class described herein, and more research is needed to establish a pervading mechanistic model of transport.

1.2 Introduction to ABC Transporters

A distinct family of membrane transporter proteins found in all life is the ATP Binding Cassette (ABC) transporter family, named from the arrangement of its domains in binding and hydrolyzing ATP [4]. ABC transporters utilize the energy released by binding and hydrolyzing ATP to perform active transport of molecules against the concentration gradient formed by the cellular membrane. ABC transporters function both as importers and exporters in prokaryotes; but only exporters are present in eukaryotes, and no known transporters are observed to translocate in both directions. ABC transporters are the largest family of proteins in the model organism *Escherichia coli* with 80 transport systems and make up approximately 5% of the species genome [5]. There are 48 ABC transporters in humans that export various classes of compounds such as lipids, cholesterol and sterols, retinoic acid metabolites, bile acids, iron complexes, nucleosides, peptides, and even antigen presentation complexes in lymphocytes [6,7]. Mutations in these proteins often manifest themselves in genetic diseases like macular degeneration, neonatal diabetes, lipid disorders, and cystic fibrosis in the case of the atypical chloride channel, ABC transporter CFTR. The extensively studied human ABC transporter P-glycoprotein (ABCB1), as well as ABCC1 and ABCG2, export large hydrophobic compounds and have been linked to multidrug resistance in tumor cells by expelling lipophilic chemotherapeutic drugs [8,9]. Prokaryotic transporters are essential to their survival and have roles in cell viability and virulence [10]. Bacterial exporters efflux various substances such as structural and cell surface compounds like lipopolysaccharides, bacterial pathogenesis proteins, peptide antibiotics, drugs, heavy metals and siderophores [11,12]. Importers are essential for the acquisition of most nutrients, from carbohydrates, amino acids and lipids, to vitamins and metal cofactors required for cell survival.

1.3 The Molecular Anatomy of ABC Transporters

All ABC transporters consist of a pair of nucleotide binding domains (NBDs, also referred to as “ABC Cassettes”) located in the cytosol, responsible for ATP hydrolysis, and a pair of transmembrane domains (TMDs) that form the translocation pathway of the substrate through the membrane (Figure 1.1). ABC importers differ from exporters in that the importer NBDs and TMDs are separate polypeptide chains, whereas prokaryotic exporters are typically homodimers of a fused TMD and NBD. Eukaryotic exporters contain all 4 domains in a single polypeptide, and currently no eukaryotic ABC importers are known to exist. Importers are tasked with nutrient uptake and osmotic balance and utilize a substrate binding protein (SBP) located in the periplasm (as opposed to membrane anchored lipoproteins in gram-positive bacteria) which are an essential component of the import system [12]. It is thus surprising that despite the different function between importers and exporters there is a high degree of homology (25-30% identity) between the ABC transporter family, particularly in the NBDs. This homology suggests a conserved mechanism in the binding and hydrolysis that powers the transport, regardless of translocation direction and structural differences in the TMDs (Figure 1.1) [11,13].

ABC transporters are categorized by their TMDs such as importer Type I, Type II, Type III (also known as Energy Coupling Factor, ECF Transporters) and exporters. Type I importers tend to have fewer transmembrane helices and arrangements then Type II importers, and their NBDs can contain a C-terminal Regulatory Domain (CRD) to regulate the rate of hydrolysis and subsequent transport. These two importer types differ from ECF transporters, which do not have complete membrane spanning domains and rely on membrane-anchored SBPs to deliver substrate. These three importer folds differ from the exporters, which are designed to pump their substrate out of the cell, and have structural differences in their channel [13]. Despite the vast differences in these TMDs, the NBDs of all ABC transporters come together to form the same “cassette-like” structure when interacting with ATP and use highly conserved catalytic cores to

power transport. Research on importers and exporters has yielded insight into the mechanism of their specific systems, as well as similarities between all ABC transporters. This introduction primarily focuses on the structure and mechanism of Type I ABC importers while emphasizing the conservation of these features throughout the different classes of ABC transporters.

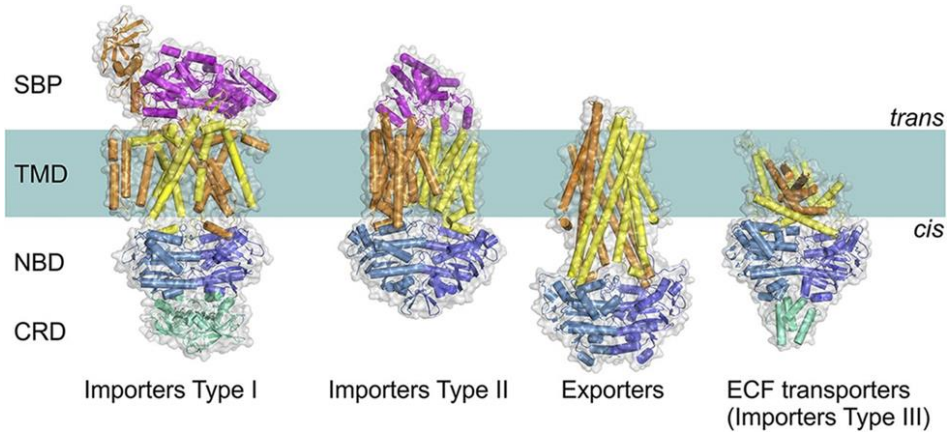

Figure 1.1: The structural anatomy of different types of ABC transporters. Notice the vast difference in TMD structure and shape (orange and yellow) and the relatively well conserved structures of the NBDs (blue). Some transporter systems use periplasmic SBPs to gather substrates (purple) while others use CRDs to regulate transport (green). This figure taken directly from [13].

1.4 ABC Transporter Nucleotide Binding Domains

The NBDs of ABC transporters can be recognized by their well-conserved ATP binding domains and catalytic cores. Both NBDs of all ABC transporters each contain two domains, the "RecA-like domain" and "α-helical domain" (Figure 1.2). The RecA-like domain owes its name from a protein fold and sequence homology to the RecA protein, which utilizes ATP in order to perform DNA recombination and repair in bacteria, but has been adapted for use in transporters over the course of evolution [14,15]. The RecA-like domain contains a "P-loop" or "Walker A" motif that binds the β-phosphate of ATP (consensus sequence GXXXXGKT/S where X is any amino acid). The "Walker B" motif (consensus sequence ϕϕϕϕD where ϕ is any hydrophobic residue)

binds the nucleotide-coordinated Mg^{2+} ion on the critical aspartate residue, as well as a glutamate residue essential for the hydrolysis of ATP. Finally, the RecA-like domain contains a “D-loop” with the sequence of EATSALD, characterized by the acidic residues at the ends of the sequence, with the glutamate involved in polarizing a catalytic water molecule and aspartate interacting with the Walker A motif [16,17]. The α-helical domain contains other conserved secondary structures known as the catalytically relevant “Q-loop,” “H motif” which provides an interface to the TMD, and the “signature sequence” (LSSGQ), involved in ATP binding to the NBDs [18].

The NBDs are oriented in a flipped “front-to-back” manner so that each end of the NBD faces the opposite side of the opposing NBD, thereby creating two ATP binding pockets that catalyze ATP hydrolysis. A single ATP binding pocket is thus composed of elements of a RecA-like domain and an α-helical domain contributed by each of the two transporter subunit NBDs. Multiple motifs described above participate in the binding of ATP with the binding pocket, resulting in pulling together the RecA-like and α-helical domains of the opposite subunits, as depicted in Figure 1.2. The RecA domain uses the Walker A motif to bind the α and β-phosphates of an ATP molecule, and the Walker B motif binds the coordinated magnesium ion while the acidic group (glutamate) acts a general base in the hydrolysis of the ATP γ-phosphate by water. On the α-helical domain of the opposite NBD, the serine residue of the ABC signature sequence LSGGQ also interacts with the ATP γ-phosphate, pulling the two NBDs together and promoting a dimerized state that can perform ATP hydrolysis [19]. The energy from binding and hydrolysis of ATP promotes conformational changes which allows substrate transport through the TMDs and across the membrane.

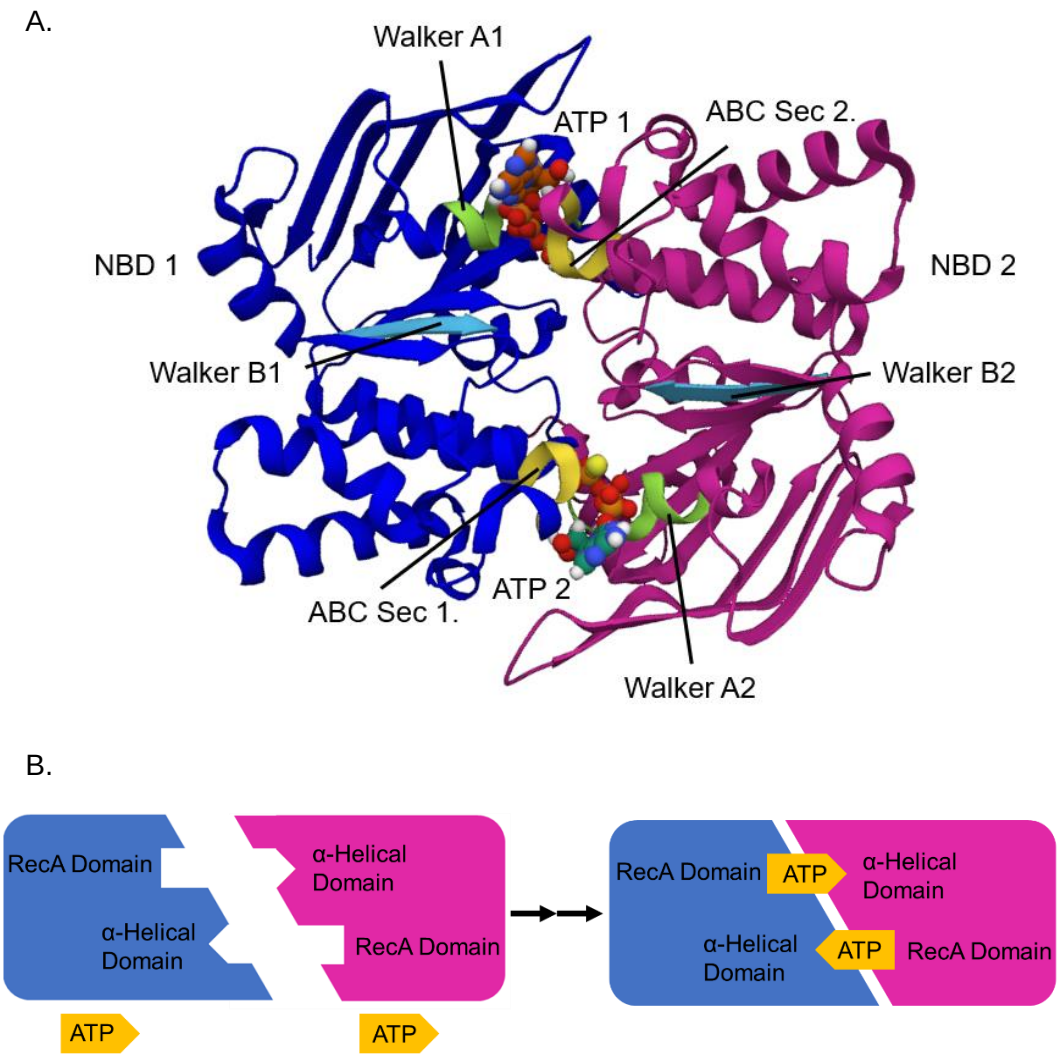

Figure 1.2: Top-down cross-section of NBDs from the crystal structure of the ABC transporter MetNI. (A) The polypeptide of NBD1 (blue) mirrors the flipped polypeptide of NBD2 (magenta). The Walker A motif (green) of the RecA domain binds ATP 1 as described, and coordinates ATP binding to the ABC signature sequence (yellow) of the α-helical domain of the opposite NBD. The Walker B motif (cyan) binds an ATP-coordinated magnesium ion (not shown) required for hydrolysis. The same domains bind ATP 2 in a flipped mirror conformation. The energy of ATP binding to the different domains causes conformational changes in the NBDs that draw them closer together in order to hydrolyze ATP. (B) A simplified schematic drawing of the two NBDs binding ATP through their respective domains. Crystal structure in (A) taken from [39].

The conformational changes exhibited by the NBDs are followed by changes in the TMDs and offer a mechanism of translocation through the channel based on the nucleotide state. Many structural and enzymatic techniques have been applied to NBDs of various ABC transporters to answer mechanistic questions such as: the stoichiometric ratio of ATP hydrolyzed to substrate translocated, how the transporter system performs transport unidirectionally without leakage in the reverse direction, and how hydrolysis is tightly coupled with transport so ATP is not needlessly wasted [20, 21]. Unfortunately, many of these important questions regarding ABC transporter function remain unanswered. Most importantly, a singular unifying mechanism of transport has not yet been elucidated for this major class of transporters. This is most intriguing considering the high level of conservation with these "molecular engines," which power the entire process. Much work remains to answer these questions if ABC transporters are to be fully understood.

1.5 ABC Transporter Transmembrane Domains

Unlike the NBDs of ABC transporters, the TMDs tend to be heterogeneous in sequence and structure to accommodate the different classes of substrates translocated. Currently ABC transporters are classified into 4 different families based on TMD folds, called Type I, Type II, Type III (ECF) and ABC exporter folds (Figure 1.3) [22]. This work primarily focuses on the structural differences of the well-studied Type I and Type II importers. Type I importers (such as the ModBC molybdate transporter, the MalFGK maltose transporter, and the MetNI methionine transporter) exhibit a minimum of 5 helices in their TMD subunits, and have four (TM2-5) helices with a similar alternating "top-to-bottom" arrangement, with the fifth helix wrapping around the outside of the channel [13, 22, 23]. The additional helices of larger Type I importers (ModBC, MalFGK) also interact with the opposing TMD subunit [18]. The Type II importer fold was first seen in the BtuCD vitamin B_{12} transporter, and is substantially larger than the Type I importers, consisting of 10 transmembrane helices in one TMD subunit, with TM2 helix positioned through the center of the subunit [24]. Type II importers lack a substrate binding pocket within the TMDs,

which is typically seen in the solved crystal structures of Type I importers. In contrast, the ABC exporter fold contains six helices and is topologically very distinct from the importer folds, as first seen in the Sav1866 multidrug exporter [25]. An important difference from importers are “long intracellular loops” that extend much further into the cytoplasm, positioning the NBDs and their interface at a greater distance from the membrane in comparison to importers. This gives the ABC exporter fold a more “tube-like” appearance (Figure 1.3). The significant differences between TMD structure, even within the same ABC transporter type, has led to many difficulties in drawing similarities between key transport events such as substrate binding, ATP hydrolysis, substrate translocation and their sequential order. The field of ABC transporters and all of their characteristics is vast and for the sake of brevity, we will focus on the mechanistical models for only ABC importers.

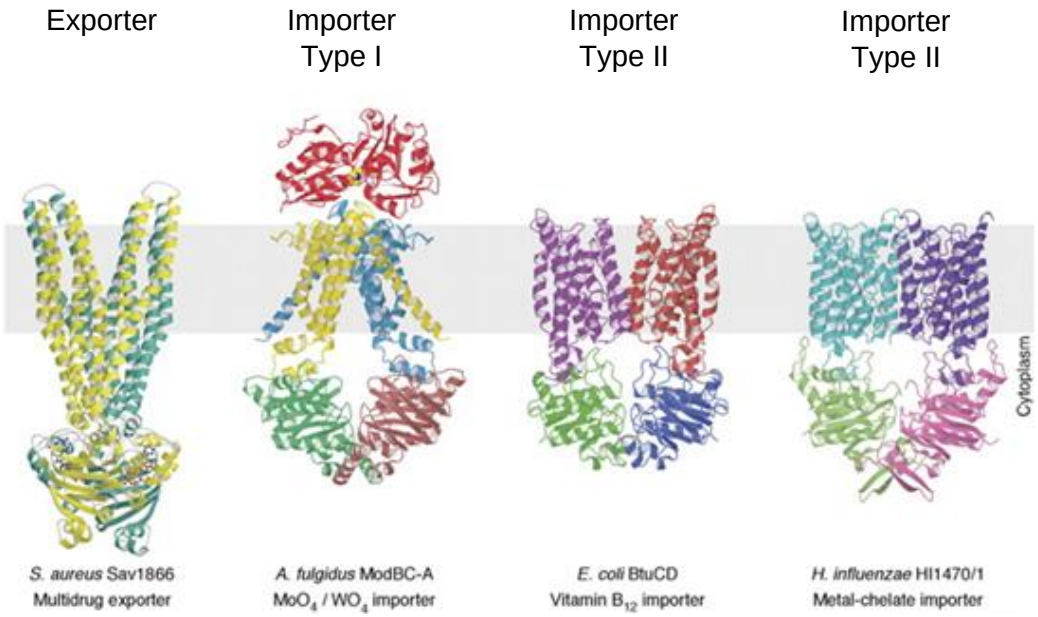

Figure 1.3 The structures of the first ABC transporters identified by their corresponding transport folds. Sav1866 TMDs are more “tube-like” in appearance in an “outward-facing” TMD orientation, as seen in most exporters. ModBC-A is a Type I importer and is more narrow in its “inward-facing” conformation. BtuCD and HI1470/1are Type II importers and are more barrel-like in their TMDs. This figure taken directly from [12].

1.6 The Alternating Access Model of Transport

The prevailing generalized model of transport is based upon structural changes in both the NBDs and the TMDs driven by the nucleotide state. The TMDs can adapt either an “outward-facing” conformation, where the TMDs are open to the extracellular or periplasmic space, or an “inward-facing” conformation, where the TMDs are open to the cytosol of the cell (Figure 1.4). The orientations of the TMDs in the outward-facing and inward-facing conformations are coupled to changes in the NBDs upon binding and hydrolysis of ATP. The NBDs are furthest from each other in the apo-nucleotide state but undergo conformational changes that align the NBD cassettes for hydrolysis upon ATP binding. Often, substrate binding to the TMD channel is required to drive hydrolysis. This coupling helps in avoiding ATP hydrolysis in the absence of substrate, thereby preventing the wasteful use of cellular energy. The nucleotide-driven conformations of the TMDs cause the opening of the channel to alternate between inward-facing and outward-facing orientations, allowing the transport of the substrate across the membrane. ATP hydrolysis and dissociation of ADP from the NBDs result in the apo-state and allows for a return to the original orientation of the protein [26]. This translocation of substrate through the cell membrane via outward-facing and inward-facing orientations of the TMDs is aptly named the “alternating access model,” and provides a highly generalized mechanistic model for the transport of ABC transporters (Figure 1.4) [18]. Here we will focus on the mechanism as it pertains to ABC importers and how the highly conserved ATPase enzymatic activity drives transport with the cognate substrate binding protein.

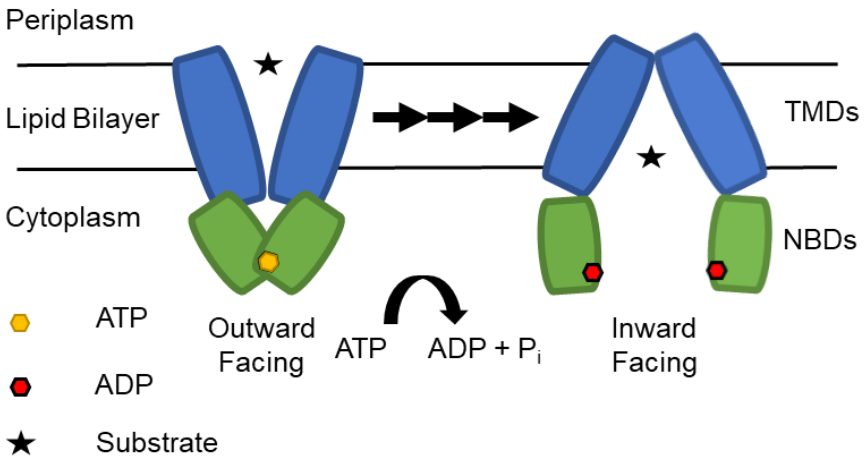

Figure 1.4: Simplified schematic of the alternating access model. Depiction of the net reaction and movement of substrate via alternating access to the channel.

1.7 The Canonical and Alternative Models of ABC Transporter Import

There are two distinct models for import in ABC transporters which differ primarily in the proposed mode of substrate delivery and the role of the substrate binding protein (SBP). In the "canonical" model (Figure 1.5A) it is proposed that substrate is first bound by the SBP and then delivered to the transporter in the apo-nucleotide state (Figure 1.5A, step 1). The binding of the SBP promotes ATP binding to the NBDs, which in turn drives NBD dimerization (Figure 1.5A, step 2). Upon ATP hydrolysis, the TMDs alternate from the outward-facing to inward-facing conformation, allowing for substrate transport through the membrane (Figure 1.5A, step 3) [26].

In the alternate "non-canonical" model (Figure 1.5B) the transporter exists in a state with a high affinity for both the SBP and ATP in the absence of substrate. In this model, the ATP-bound transporter is in the outward-facing conformation. The unliganded SBP then binds the transporter, forming a transporter-SBP complex without substrate (Figure 1.5B, step 1). This complex contains a channel through the SBP that allows the substrate to enter the permeation pathway formed by

the TMDs (Figure 1.5B, step 2). Substrate entry triggers ATP hydrolysis, and the TMDs conformationally rearrange to an inward-facing conformation to drive substrate transport (Figure 1.5B, step 3) [22]. In both models, it is assumed that ADP dissociation drives a return to the original confirmation for another cycle of transport. The order of substrate and ATP binding has been debated with some evidence that ATP binding may increase the binding affinity for substrate, then triggering the required conformation for hydrolysis and transport [18]. Others have postulated that the energetically favorable step of ATP binding is the step that allows the TMDs to perform translocation, with the energy released from ATP hydrolysis driving the later steps of the mechanism [27].

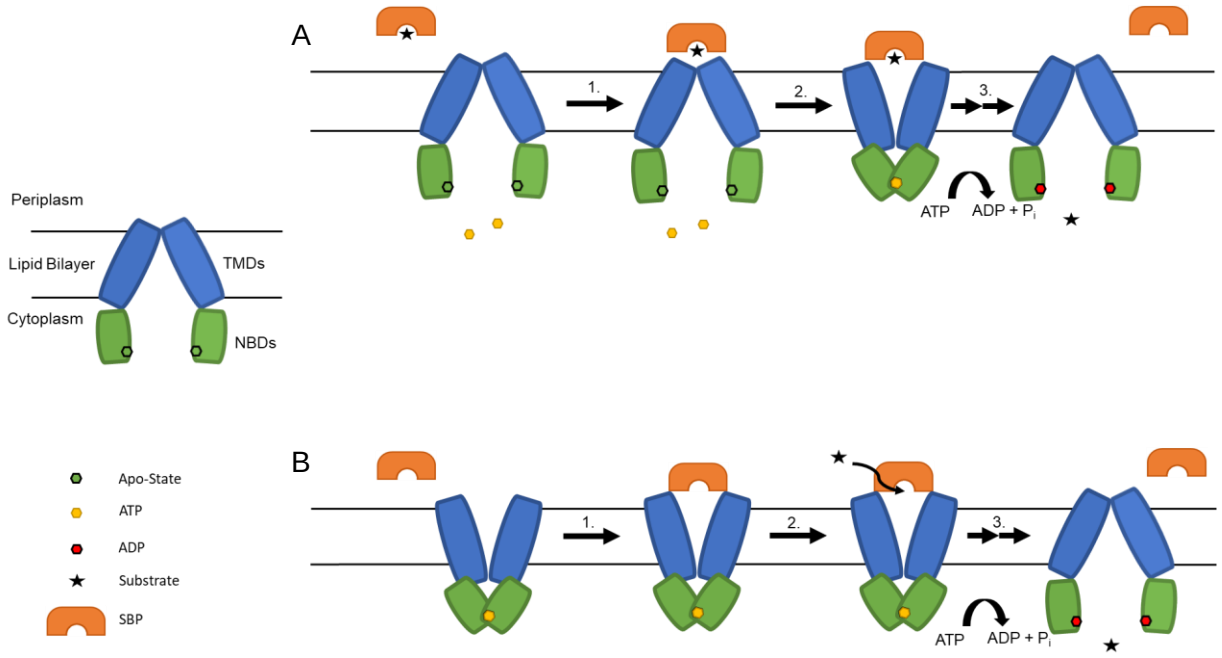

Figure 1.5. Simplified schematic of two hypothesized modes of import TMDs are depicted in blue, the NBDs in green, the SBP in orange, the substrate as a star, ATP yellow and ADP red. A biological membrane is depicted as parallel lines. Double arrows indicate numerous possible steps within the mechanism. (A) The canonical pathway. An inward-facing transporter awaits the docking of a substrate-bound SBP (step 1). After the SBP binds, ATP binding triggers NBD dimerization which in turns drives rearrangement of the TMDS to the outward-facing conformation (step 2). Substrate is released from the SBP, ATP is hydrolyzed, and the substrate is translocated through the channel formed from a now outward-facing conformation (step 3). Eventually the SBP, ADP and substrate are released and the transporter is ready to repeat the process after returning to an inward-facing conformation (B) The non-canonical pathway**.** After ATP binding, an outward-facing transporter binds with a substrate-free SBP (step 1). The binding of the SBP to TMDs increases the transporter-SBP affinity for the substrate, which then passes through a channel in the SBP (step 2). Once substrate is bound, ATP is hydrolyzed, triggering the rearrangement to the inward-facing conformation and passage of the substrate through the membrane (step 3). Following ADP release and substrate translocation, the SBP may or may not disassociate before the next cycle.

1.8 Discovery of the *E. coli* Methionine Importer MetNI

While the structures of several importers have been investigated in great detail to elucidate the mechanism of ABC transporters, the *E. coli* methionine importer system provides a unique case to study the functionality of Type I importers. MetNI is a Type I ABC transporter responsible for the uptake of D- and L-methionine against a concentration gradient. MetNI shuttles methionine from the periplasmic space into the cytosol in order to maintain intracellular methionine pools. Previous studies by Kadner were able to identify two methionine transport systems in *E. coli*, a high affinity system (K_M = 0.075 μM) and low affinity system (K_M = 40 μM). These *in vivo* studies relied on mutant strains, particularly those with mutations in the *metD* and *metP* gene loci [28,29]. Whereas wild-type *metD* strains supported transport of both L- and D-methionine, strains mutant in the *metD* locus resulted in the loss of high affinity L-methionine transport as well as D-methionine uptake. *MetD* gene products were also capable of transporting methionine derivatives such as seleno-methionine [28,29]. Furthermore, the uptake of L-methionine was not outcompeted by other amino acids at mM concentrations [28]. The *metP* locus was shown to be responsible for the low affinity uptake of L-methionine, and a double mutant in the *metD* and *metP* loci was shown to be defective in transport of both isomers of methionine [28].

1.9 Regulation of Methionine Import *In Vivo* (Identification of the Cognate *E. coli* Methionine Binding Protein MetQ)

Most bacterial transport systems have been shown to be regulated by their controlled expression, except for some cases of sugar uptake where activity is regulated by the concentration of internal metabolites, or by other transporters [30]. However, of the bacterial amino acid transporters characterized, repression was inferred to be the result of a decreased amount of substrate binding protein (such as in the case of the leucine transporter) without evidence of a regulatory gene [31]. This is in direct contrast to the study of transport systems of

fungal species such as *Penecillium* and *Neurospera crassa,* which are controlled by genetic regulation that affects the synthesis of required proteins and by kinetic inhibition of the rate of influx by the amount of internal substrate [32, 33]. In the case of methionine transport in *E. coli*, the internal L-methionine pool significantly regulates the kinetics of methionine uptake [30]. By carefully measuring uptake rates of radioactive L-methionine in the presence of varying internal L-methionine pools, Kadner and colleagues were able to deduce that the high affinity transport exhibits a form of regulation called “transinhibition” [29]. Transinhibition refers to the inhibition of the influx rate in a transport system caused by high intracellular levels of the transported material. This phenomenon has been of unique interest of the *E. coli* methionine ABC importer system since its discovery, and these early findings foreshadowed the elucidation of an allosteric mechanism of methionine transport regulation over 30 years later [34].

1.10 Identification of the *metD* Locus Encoding for the MetNIQ System

The *metD* locus was originally proposed to be composed of six gene candidates: *abc, yaeC, yaeB, yaeD, yaeE, and yaeF* [35]. The *metD* locus encoding the “MetD” transporter system was found to contain a Walker A motif, the “ABC signature” linker peptide and the Walker B motif within the gene *abc.* The *yaeE* and *yaeC* genes encode for a permease and a methionine binding domain, respectively. *YaeB* displays no defining features when analyzed relative to the SwissPro protein structure database, while *yaeD* and *yae*F were characterized as a hexose 1,7-bisphosphate phosphatase and a lipoprotein, respectively [35]. Merlin and colleagues selectively ablated each gene, and the individual strains exhibited growth in the presence of L-methionine due to the presence of the *metP* locus. However, when the deletion strains were grown in D-methionine as the sole methionine source, only strains with active *metD* transport were viable. Under these conditions, growth inhibition was observed in the *Δabc, ΔyaeC and ΔyaeE* deleted strains, confirming the role of their gene products as the functional components of the *metD* locus

[35]. The genes were subsequently renamed *metN*, *metI*, and *metQ* encoding the ATPase, transmembrane domain, and the substrate binding protein, respectively [35, 36].

1.11 The MetNI Crystal Structure

The ABC transporter component of the "MetD system," MetNI, was successfully crystallized and resolved to 3.7 Å in 2008 [37]. The crystallized transporter contained two MetN NBD polypeptides and two MetI TMD polypetides. The four polypeptides were arranged in an inward-facing conformation (Figure 1.6). When compared to the crystal structures of previously studied bacterial ABC transporters, such as ModBC and MalFGK, MetNI has smaller transmembrane domains, consisting only of five transmembrane helices per MetI monomer. The MetNI NBDs were set apart in a wide inward-facing conformation, with approximately 30 Å between the signature motifs of opposing NBDs. Later the resolution was increased to 2.9 Å using the detergent cyclohexyl-pentyl-β-d-maltoside (CY5) which improved the structural model, corrected the sequence, and identified ADP in the nucleotide binding site while in the inward-facing conformation [38].

Additionally, there was a C-terminal extension on each MetN that had not been seen in other transporters. These extensions, termed C2 domains, appeared to sterically separate the NBDs in the crystal structure. Each C2 domain contains an ACT domain, a protein domain found in many metabolic enzymes that are regulated by the concentration of amino acids. When soaked with L-selenomethionine, two binding sites were discovered near the dimer interface of the C2 domains, as observed in other ACT domain proteins inhibited by their corresponding ligands. Importantly, the presence of this ACT domain suggested a potential explanation for the transinhibition phenomenon observed by Kadner. When intracellular concentrations of L-methionine are high, the ACT domains bind L-methionine and drive the dimerization of the C2 domains. In turn, the dimerized C2 domains drive the NBDs apart. This separation prevents ATP

binding and hydrolysis at the NBD interface, which results in the locking of the transporter in the inward-facing conformation. Ultimately, transport is inhibited.

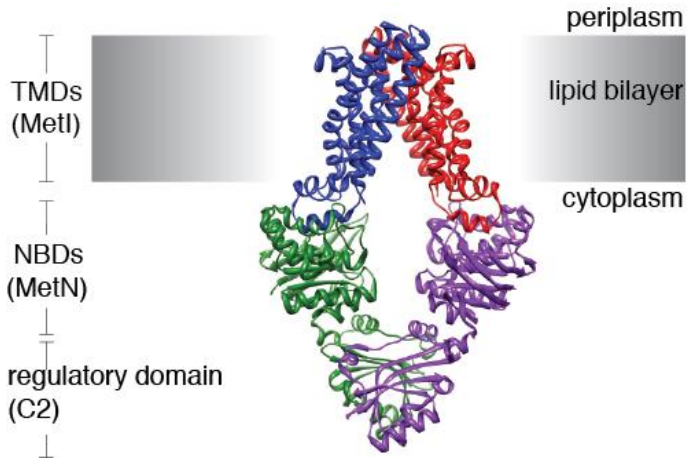

Figure 1.6 The crystal structure of MetNI. The structure of MetNI with each polypeptide chain colored differently. This figure is taken directly from [37].

1.12 Inhibition-deficient MetNI Mutants

In the same study, L-methionine was shown to inhibit MetNI ATPase activity, with the apparent half maximum inhibition constant (K_I) of approximately 30 µM. High concentrations of D-methionine had no effect on ATPase activity, while L-selenomethionine was a more potent inhibitor with K_I = 10 µM [37]. A mutant MetN construct, lacking the regulatory C2 domains, lost the inhibitory effect triggered by L-methionine, providing further evidence in favor of the transinhibition model described above. Although these ATPase assays did not directly measure substrate transport, they provided evidence that the C2 domains were responsible for the observed L-methionine-dependent ATPase inhibition [37]. Later, a mutation in the C2 domain at residue N295 was found to reduce binding of L-methionine to near undetectable levels by

isothermal titration calorimetry, rendering a mutant of MetNI that is theoretically uninhibited by the ligand at cytoplasmic levels [39].

1.13 Allosteric Regulation of MetNI

The regulatory mechanism of MetNI via transinhibition was studied in greater detail using kinetic and thermodynamic assays [34]. Using ATPase assays, MetNI was shown to have a $K_{M(ATP)}$ of 330 ± 20 μM and a Hill coefficient of 1.7 ± 0.1, revealing positive cooperativity between the two ATP binding sites, a trait observed in other ABC transporters [21,40-42]. L-methionine inhibited ATPase activity with a $K_{I(\text{L-Met})}$ of 41 ± 1 μM and a Hill coefficient of 1.4 ± 0.1, suggesting the presence of more than one methionine binding site and a weak cooperativity between them. In the presence of increasing L-methionine concentrations, the V_{max} decreased, and the $K_{M(ATP)}$ remained relatively constant, indicating that L-methionine was indeed a noncompetitive inhibitor of MetNI ATPase activity. Using isothermal titration calorimetry, it was determined that MetNI bound L-Met with a $K_{D(\text{L-Met})}$ of 33 ± 4 μM, a value close to $K_{I(\text{L-Met})}$ for MetNI [34]. Furthermore, binding studies measured 2.2 ± 0.1 L-methionine binding sites per transporter, consistent with both kinetic and structural studies. These results confirmed Kadner's observation that transinhibition is linked to the allosteric regulation of MetNI's ATPase activity and therefore regulates the import of methionine [28,29].

1.14 The MetNI-MetQ Complex

One key component of the MetNI transport system was purposefully omitted from the work published by Yang, et al. [34]. The periplasmic substrate binding protein MetQ was excluded from functional studies in order to reduce complications due to the additional L-methionine that co-purifies with MetQ [38]. Like other ABC import systems, MetQ binds its preferred substrate very tightly, and thus co-purifies with L-methionine tightly bound ($K_D << 1$ μM) [43, 44]. The SBP is a key component of transport however, and crystal structures of transporters complexed with their

cognate importers have aided in in establishing the basic steps of transport, particularly in the Type I MalFGK and Type II BtuCD importers [45, 46]. The importance the SBP plays in its cognate transport system necessitates determining the crystal structure of other SBPs regardless of importer type. Thus, efforts were focused on solving the crystal structure of the MetNI transporter in complex with the MetQ SBP.

Attempts were made to stabilize the MetNI-MetQ complex using a variety of nucleotide states and mutations [47]. Complex formation was initially assessed qualitatively via gel filtration and blue native polyacrylamide gel electrophoresis (BN-PAGE). The most promising conditions to form a stable MetNIQ complex consisted of: a catalytically inactive mutant of MetNI, a mutant of MetQ with decreased affinity for L-methionine, and ATP with EDTA, the latter which chelates Mg^{2+} and prevents ATP hydrolysis. Quantitative analyses showed that ligand-free MetQ forms a higher affinity complex with MetNI than does L-Met-loaded MetQ, in direct contrast to the maltose transporter, which requires its liganded SBP to form a stable complex [23, 47]. The study revealed conditions that could support crystallization of an intermediate state in the transport cycle, and provided new clues as to the methionine transport mechanism [45-48].

1.15 Limitations of Detergent-Solubilized ABC Transporters

ABC transporters, like other membrane proteins, are most often studied in detergent micelles. While the lipid bilayer is the preferred environment for these proteins, biochemical purification requires solubilization of the membrane using commercially-available synthetic detergents. Unfortunately, detergent micelles may alter the conformational changes of membrane proteins by altering the energetic costs of conformations that are unfavorable in the native lipid environment of a membrane [49,50]. Thus, micelles may create an artificial environment that is not a faithful mimic of the lipid membrane. As a result, notable changes in function have been observed in ABC transporters depending on the method of solubilization, such as decreased rates

of ATP hydrolysis upon reconstitution into proteoliposomes [50,51]. Similar to MetNI, many detergent-solubilized ABC transporters show basal ATPase activity in the absence of substrate [52]. This uncoupled *in vitro* activity is unintuitive from an evolutionary perspective, where ATP expenditure by ABC transporters should be minimized and should only occur in the presence of substrate. When reconstituted in proteoliposomes, both the Type I importer MalFGK and the Type II importer BtuCD show greatly decreased basal ATPase activity [52,53].

There has been a shift to study ABC transporters in more physiologically relevant lipid environments in order to overcome the potential structural deformations that detergent micelles may impose. Proteoliposomes have several caveats, particularly with respect to the directionality of insertion into the membrane, as transporters can be reconstituted both “inside-out” and “right-side in.” This complication provides an additional variable in an already complex system. It is also difficult to produce monodisperse homogeneous populations of proteoliposomes required for functional studies. Lastly, reconstitution of transporter into proteoliposomes is costly and often varies in yield. Alternate systems have been investigated to better mimic the lipid membrane without the limitations and challenges of vesicle-based ABC transporters, as described below.

1.16 Protein-Lipid Nanodiscs

One promising alternative to liposomes is the use of “nanodiscs,” a nanoscale discoidal bilayer of polar lipids encircled by an amphipathic scaffold of proteins (Figure 1.7). The individual protein components self-assemble into a dimeric ring in the presence of phospholipids, enclosing a phospholipid bilayer between a disc of two stacked identical proteins. Nanodiscs provide a tractable alternative to detergent micelles, and self-assembly into nanodiscs allows for solubilization of nonpolar and amphipathic molecules into monodisperse solutions [54]. Nanodiscs have become a well-established tool in the world of membrane proteins due to their defined size, composition, and stability.

The amphipathic helical protein responsible for assembling the nanodisc are called membrane scaffold proteins (MSP). The MSPs are derived from the human apolipoprotein ApoA1 and are modified to maintain a uniform discoidal shape, rather than spherical lipoprotein particles found *in vivo* (Figure 1.7). The MSPs are surprisingly resistant to aggregation and compatible with many different mixtures of polar phospholipids, though specific parameters seem to vary based on the membrane protein of interest [55]. Different variants of the MSP have been made to accommodate the size of different membrane proteins, with deletions or extensions in the helical sequence resulting in smaller and larger nanodiscs, respectively. Nanodiscs formed from the MSP1D1 variant of the protein have the smallest diameter and accommodate more narrow transmembrane domains. To accommodate larger membrane proteins, MSP1E3 variant proteins are extended to provide a larger area of membrane for reconstitution of membrane proteins or complexes (Figure 1.7). Ever since a functionally active mouse P-glycoprotein transporter was reconstituted into a nanodisc [56], nanodiscs have been utilized in structural, functional, and regulatory studies of different importer systems [57,58]. Nanodiscs have also been cited as a practical alternative to detergents for ABC transporter purification [59]. The MSP nanodisc proteins used in this study to reconstitute MetNI methionine transporter are MSP1D1 and MSP1E3 nanodiscs (Figure 1.7)

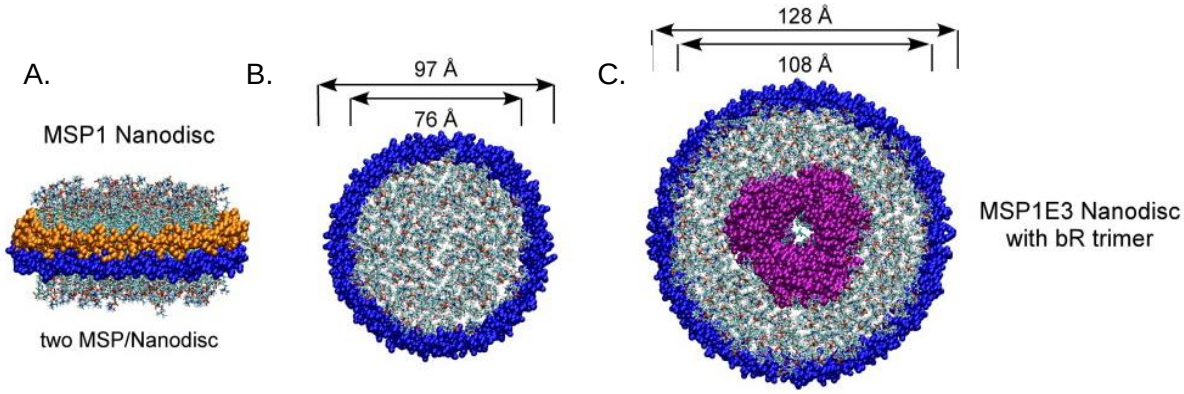

Figure 1.7 Illustration of intact dimeric MSP nanodiscs. (A) Side view of a nanodisc with two MSP1D1 proteins per single nanodisc. (B) Top view with the diameter of the lipid bilayer and scaffold protein in Angstroms, Å. (C) Top view of a MSP1E3 nanodisc containing reconstituted Bacteriorhodpsin (bR) trimer. This figure is taken directly from [55].

1.17 Nanodiscs as an Alternative Membrane Environment for MetNI

Observed differences between detergent-solubilized and membrane-embedded ABC transporters have been reported due to the structural implications of the membrane environment as described in section 1.15. These inconsistencies interfere with devising accurate mechanisms of transport when the results of one membrane environment can contradict another. One goal of this research was to test a reconstitution approach for MetNI that could provide a more faithful mimic of the lipid bilayer environment. Here we test the hypothesis that the assembly of purified MetNI transporter into a soluble phospholipid bilayer nanodiscs results in a more native environment, evaluated by the level of basal ATP hydrolysis when compared with detergent-solubilized MetNI.

1.18 Research Summary

Here I describe the successful reconstitution of the MetNI transporter in two different MSP nanodisc systems (MSP1D1 and MSP1E3D1). The reconstitution and confirmation of MetNI into nanodiscs proved exceptionally challenging and required several reorganizations in approach. Once the successful reconstitution of MetNI was confirmed via multiple tests, protocols were then repeatedly optimized to maximize reconstitution yield and homogeneity. Next, I present initial kinetic and thermodynamic measurements of enzymatic activity and affinity of the substrate binding protein using reconstituted MetNI nanodiscs. These initial findings are promising and define future research goals for understanding the MetNIQ transporter mechanism.

1.19 References

[1] Neijsel O.M.; Teixeira de Mattos M.J.; Tempest DW. Escherichia coli and Salmonella: *Cellular and Molecular Biology* **1996**, pp. 1283–1692.

[2] Stouthamer A.H. The search for correlation between theoretical and experimental growth yields. *Internal Reviews Biochem* **1979**, 21:1–47.

[3] Skou J. C. The Identification of the Sodium-Potassium Pump (Nobel Lecture). *Angewandte Chemie (International Ed. in English)* **1998**, 37(17): 2320–2328.

[4] Higgins C.F. ABC Transporters: From Microorganisms to Man.; *Annual Review of Cell Biology* **1992**, 8 (1): 67-113.

[5] Linton, K.J; Higgins, C.F. The *Escherichia coli* ATP-binding cassette (ABC) proteins. *Molecular Microbiology* **1998**, 28: 5-13.

[6] Wilkens S. Structure and mechanism of ABC transporters. *F1000 Prime Rep* **2015**, 3: 7-14.

[7] Leone, P.; MHC Class I Antigen Processing and Presenting Machinery: Organization, Function, and Defects in Tumor Cells, *Journal of the National Cancer Institute* **2013**, 10516,21,1172–1187.

[8] Gottesman M.; Pastan I.; Ambudkar S. P-glycoprotein and multidrug resistance. *Current Opinion in Genetic Development* 1**996**, 6(5): 610-617.

[9] Sharom F. J. ABC multidrug transporters: structure, function and role in chemoresistance. *Pharmacogenomics* **2008**, 9(1): 105–127.

[10] Davidson, A.; Chen, J. ATP-binding cassette transporters in bacteria. *Annual Review of Biochemistry* **2004**, 73: 241–268.

[11] Dassa, E.; Bouige, P. The ABC of ABCs: A phylogenetic and functional classification of ABC systems in living organisms. *Research in Microbiology*. **2001**, 2508 (01) 01194-9.

[12] Hollenstein, K.; Frei, D.; Locher, K. Structure of an ABC transporter in complex with its binding protein *Nature* **2007**, 446, 213–216.

[13] Beek, J.; Guskov, A.; Slotboom, D. J. Structural diversity of ABC transporters. *The Journal of General Physiology* **2014**, 143(4): 419–435.

[14] Chen, J.; Lu, G.; Lin, J.; Davidson, A. L.; Quiocho, F. A. A tweezers-like motion of the ATP-binding cassette dimer in an ABC transport cycle. *Molecular Cell* **2003**, 12(3), 651–661.

[15] Cox M. M. Regulation of bacterial RecA protein function. *Critical Reviews in Biochemistry and molecular biology* **2007**, *42* (1), 41–63.

[16] Ambudkar, S. V.; Kim, I. W.; Xia, D.; Sauna, Z. E. The A-loop, a novel conserved aromatic acid subdomain upstream of the Walker A motif in ABC transporters, is critical for ATP binding. *FEBS Letters* **2006**, 580(4), 1049–1055.

[17] Jones, P. M.; George, A. M. Role of the D-loops in allosteric control of ATP hydrolysis in an ABC transporter. *The Journal of Physical Chemistry* **2012**, *116*(11), 3004–3013.

[18] Rees, D.; Johnson, E.; Lewinson, O. ABC transporters: The power to change. *Nature Reviews, Molecular Cell Biology* **2009**, 15334406.

[19] Geourjon, C.; Orelle, C.; Steinfels, E.; Blanchet, C.; Deléage, G.; Pietro, A. D.; Jault, J.-M. A common mechanism for ATP hydrolysis in ABC transporter and helicase superfamilies. *Trends in Biochemical Sciences* **2001**, 26(9), 539–544.

[20] Patzlaff, J. S.; van der Heide, T.; Poolman, B. The ATP/substrate stoichiometry of the ATP-binding cassette (ABC) transporter OpuA. *The Journal of Biological Chemistry* **2003**, 278(32), 29546–29551

[21] Korkhov, V. M.; Mireku, S. A.; Locher, K. P. Structure of AMP-PNP-bound vitamin B12 transporter BtuCD-F. *Nature* **2012**, 490(7420), 367–372.

[22] Locher, K. Structure and mechanism of ABC transporters. *Current Opinion in Structural Biology* **2004**, 14(4): 426–431

[23] Oldham, M. et al. Crystal structure of a catalytic intermediate of the maltose transporter. *Nature* **2007**, 450(7169), 515–521.

[24] Locher, K.; Lee, A.; Rees, D. The E. coli BtuCD structure: a framework for ABC transporter architecture and mechanism. *Science* **2002**, 296 (5570), 1091–1098.

[25] Dawson, R.; Locher, K. Structure of a bacterial multidrug ABC transporter. *Nature* **2006**, 443(7108), 180–185.

[26] Jardetzky, O. Simple allosteric model for membrane pumps. *Nature* **1966**, 211:969-970.

[27] Fiorentino, F.; Bolla, J.; Mehmood, S.; et. al. The Different Effects of Substrates and Nucleotides on the Complex Formation of ABC Transporters. *Structure* **2019**, 27(4), 651–659.e3.

[28] Kadner R. Transport systems for L-methionine in Escherichia coli. *Journal of Bacteriology* **1974**, 117(1), 232–241.

[29] Kadner R. Regulation of methionine transport activity in Escherichia coli. *Journal of Bacteriology* **1975**, 122(1), 110–119.

[30] Kornberg H. Carbohydrate transport by micro-organisms. *Proceedings of the Royal Society of London. Series B, Biological Sciences* **1973**, 183(1071), 105–123.

[31] Penrose W.; Nichoalds G.; et al. Purification and Properties of a Leucine-binding Protein from Escherichia coli *Journal of Biological Chemistry* **1968**, 243 p. 5921.

[32] Benko, P. V.; Wood, T. C.; Segel, I. H. Multiplicity and regulation of amino acid transport in Penicillium chrysogenum. *Archives of Biochemistry and Biophysics* **1969**, 129(2), 498–508.

[33] Cuppoletti, J.; Segel, I. Transinhibition kinetics of the sulfate transport system of Penicillium notatum: analysis based on an iso uni uni velocity equation. *The Journal of Membrane Biology* **1974**, 17(3), 239–252.

[34] Yang, J. G.; Rees, D. C. The allosteric regulatory mechanism of the Escherichia coli MetNI methionine ATP binding cassette (ABC) transporter. *The Journal of Biological Chemistry* **2015**, 290(14), 9135–9140.

[35] Merlin, C.; Gardiner, G.; et al. The Escherichia coli metD locus encodes an ABC transporter which includes Abc (MetN), YaeE (MetI), and YaeC (MetQ). *Journal of Bacteriology* **2002**, 184(19), 5513–5517.

[36] Gál, J.; Szvetnik, A.; Schnell, R.; Kálmán, M. The metD D-methionine transporter locus of Escherichia coli is an ABC transporter gene cluster. *Journal of Bacteriology* **2002**, 184(17), 4930–4932.

[37] Kadaba, N. et al. The high-affinity E. coli methionine ABC transporter: structure and allosteric regulation. *Science* **2008**, 321(5886), 250–253.

[38] Johnson, E.; Nguyen, P. T.; Yeates, T. O.; Rees, D. C. Inward-facing conformations of the MetNI methionine ABC transporter: Implications for the mechanism of transinhibition. *Protein science: a publication of the Protein Society* **2012**, 21(1), 84–96.

[39] Nguyen, P. T.; Lai, J. Y.; Lee, A. T.; Kaiser, J. T.; Rees, D. C. Noncanonical role for the binding protein in substrate uptake by the MetNI methionine ATP Binding Cassette (ABC) transporter. *Proceedings of the National Academy of Sciences of the United States of America* **2018**,*115*(45), E10596–E10604

[40] Tal, N.; Ovcharenko, E.; Lewinson, O. A single intact ATPase site of the ABC transporter BtuCD drives 5% transport activity yet supports full in vivo vitamin B12 utilization. *Proceedings of the National Academy of Sciences of the United States of America* **2013** 110(14), 5434–5439.

[41] Davidson A.; Laghaeian S.; Mannering DE. The maltose transport system of Escherichia coli displays positive cooperativity in ATP hydrolysis. *Journal of Biological Chemistry* **1996**, 271:4858–4863.

[42] Liu, C.; Liu, P.; Ames, G. Characterization of the adenosine triphosphatase activity of the periplasmic histidine permease, a traffic ATPase (ABC transporter). *The Journal of Biological Chemistry* **1997**, 272(35), 21883–21891.

[43] Deka, R. K.; Neil, L.; K. E.; Machius, M.; Tomchick, D. R.; Brautigam, C. A.; Norgard, M. V. Structural evidence that the 32-kilodalton lipoprotein (Tp32) of Treponema pallidum is an L-methionine-binding protein. *The Journal of Biological Chemistry* **2004**, 279(53), 55644–55650.

[44] Williams W.; Zhang R.; Zhou M.; Joachimiak G.; Gornicki P.; Missiakas D.; Joachimiak A. The membrane-associated lipoprotein-9 GmpC from Staphylococcus aureus binds the dipeptide GlyMet via side chain interactions. *Biochemistry* **2004**, 43:16193–16202.

[45] Oldham, M.; Chen, J. Crystal structure of the maltose transporter in a pretranslocation intermediate state. *Science* **2011**, 332(6034), 1202–1205.

[46] Korkhov, V.; Mireku, S.; Veprintsev, D. et al. Structure of AMP-PNP–bound BtuCD and mechanism of ATP-powered vitamin B12 transport by BtuCD–F. *Nature Structural and Molecular Biology* **2014**, 21: 1097–1099.

[47] Nguyen, P.; Li, Q.; Kadaba, N.; Lai, J.; Yang, J.; Rees, D. The contribution of methionine to the stability of the Escherichia coli MetNIQ ABC transporter-substrate binding protein complex. *Biological Chemistry* **2015**, 396(9-10): 1127–1134.

[48] Chen, J.; Sharma S.; Quiocho F.; Davidson A. Trapping the transition state of an ATP-binding cassette transporter: Evidence for a concerted mechanism of maltose transport. *Proceedings of the National Academy of Sciences* **2001**, 98(4): 1525-1530.

[49] Phillips, R.; Ursell, T.; Wiggins, P.; Sens, P. Emerging roles for lipids in shaping membrane-protein function. *Nature* **2009**, 459(7245): 379–385.

[50] Rice, A. J.; Alvarez, F. J.; Davidson, A.; Pinkett, H. Effects of lipid environment on the conformational changes of an ABC importer. *Channels* **2014***,* 8(4), 327–333.

[51] Borths, E. L.; Poolman, B.; Hvorup, R. N.; Locher, K. P.; Rees, D. C. In vitro functional characterization of BtuCD-F, the Escherichia coli ABC transporter for vitamin B12 uptake. *Biochemistry*, **2005,** 44(49), 16301–16309.

[52] Reich-Slotky, R.; Panagiotidis, C.; Reyes, M.; Shuman, H.; The detergent-soluble maltose transporter is activated by maltose binding protein and verapamil. *Journal of Bacteriology* **2000**, 182(4), 993–1000.

[53] Alvarez, F.; Orelle, C.; Huang, Y.; Bajaj, R.; Everly, R.; Klug, C.; and Davidson, A. Maltose-bound MBP stabilizes a semi-open ABC dimer. *Molecular Microbiology* **2015**, 98: 878-894.

[54] Denisov, I.; Sligar, S. Nanodiscs in Membrane Biochemistry and Biophysics. *Chemical Reviews* **2017**, 117(6), 4669–4713.

[55] Bayburt, T.; Sligar, S.; Membrane protein assembly into Nanodiscs. *FEBS Letters*, **2010**, 584(9), 1721–1727.

[56] Ritchie, T.; Grinkova, Y.; Bayburt, T.; Denisov, I.; Zolnerciks, J.; Atkins, W.; Sligar, S. Reconstitution of membrane proteins in phospholipid bilayer nanodiscs. *Methods in Enzymology* **2009,** 464: 211–231.

[57] Bao, H.; Duong, F. **2012.** Discovery of an auto-regulation mechanism for the maltose ABC transporter MalFGK2*. PLoS ONE* **2012,** 7(4): E34836.

[58] Takeaki, K.; Caaveiro, J.; Ryota, A.; Toyomasa K.; Kouhei T.; Catalytic activity of MsbA reconstituted in nanodisc particles is modulated by remote interactions with the bilayer, *FEBS Letters* **2011,** 585 (22), 3533-3537.

[59] Gulati, S.; Jamshad, M.; Knowles, T.; Morrison, K.; Downing, R.; Cant, N.; Collins, R.; Koenderink, J.; Ford, R.; Overduin, M.; Kerr, I.; Dafforn, T.; Rothnie, A.; Detergent-free purification of ABC (ATP-binding-cassette) transporters. *The Biochemical Journal* **2014***,* 461(2), 269–278.

Chapter 2. Purification of Components for Nanodisc Assemblies and Analysis

2.1 Recombinant DNA Plasmids and Transformation

DNA plasmids encoding the following proteins were kindly provided by Douglas Rees (California Institute of Technology). 10x-polyhistidine-tagged wild-type MetNI, E166Q MetNI, and N295A MetNI were encoded in a pET19b vector. DNA plasmids encoding the MSP1D1 and MSP1E3D1 were kindly provided by Frank Duong (University of British Columbia). Wild-type MetQ and N229A MetQ including the signal sequence and a 6x-polyhistidine tag were encoded in a pET21b vector. A FLAG-tagged version of MetNI was also provided on a pET19b plasmid. 7x-polyhistidine-tagged versions of MSP1D1 and MSP1E3D1 were encoded in pET28a plasmids. All microbial culture was carried out with sterile equipment, media, and under a flame unless otherwise noted. All plasmids were transformed in *E. coli* DH5α cells (Invitrogen). Transformants were selected for using 50 µg/mL kanamycin for MSP plasmids and 100 µg/mL ampicillin for all other plasmids. DNA was extracted from overnight 5 mL cultures using a Wizard® Plus SV Miniprep Kit (Promega).

2.2 Expression of MetNI, MetQ, and MSP Proteins

Plasmids were expressed in *E. coli* BL21-Gold (DE3) cells (Agilent). All MetNI constructs were expressed as previously described with slight variations [1]. 5 mL starter cultures of lysogeny broth (1% tryptone, 1% NaCl, 0.5% yeast extract, autoclaved) were inoculated with a single colony of transformed BL21-Gold (DE3) cells and incubated at 37°C with shaking at 225 rpm until flocculent (approximately 5 hours). Starter culture was added to make a 1 L large-scale culture with a final optical density of 0.01 at 600 nm. Four 1 L cultures were grown in Terrific Broth (24 g/L yeast extract, 12 g/L tryptone, 72 mM K_2HPO_4, 17 mM KH_2PO_4 and 0.5% glycerol, autoclaved) with 100 µg/mL ampicillin. Large-scale cultures were grown at 37˚C with shaking at 180 rpm. When the OD 600 reached 4.0, protein expression was induced with 1 mM IPTG for 2 hours.

Cultures were pelleted via centrifugation at 39,175 x g for 20 minutes at 4°C and stored at -80°C. MSP1D1 and MSP1E3D1 were expressed in the same manner except with 50 µg/mL kanamycin instead of ampicillin.

Wild-type MetQ and N229A MetQ were expressed using the auto induction media ZYM-5052 as previously described [2]. ZYM-5052 media consists of 1% tryptone, 0.5% yeast extract, 0.5 % glycerol, 0.05 % glucose, 0.2 % α-lactose, 25 mM Na_2HPO_4, 25 mM KH_2PO_4, 50 mM NH_4Cl, 5 mM Na_2SO_4, and 1 mM $MgSO_4$. Additionally, 200 µL of a "Trace Metals" solution (50 mM $FeCl_3$, 20 mM $CaCl_2$, 10 mM $MnCl_2$, 10 mM $ZnSO_4$, 2 mM $CoCl_2$, 2 mM $CuCl_2$, 2 mM $NiCl_2$, 2 mM Na_2MoO_4, 2 mM Na_2SeO_3, 2 mM H_3BO_3) was added to each culture. It should be noted that the trace metals solution was tested to have no appreciable effect on growth or expression and was deemed unnecessary in later cultures (data not shown). A single flocculent 5 mL LB starter culture of transformed BL21-Gold (DE3) cells were added to 1 L of auto induction media containing 100 µg/mL ampicillin. Cultures were incubated at 37°C overnight with shaking at 180 rpm. The following morning, approximately 16-20 hours later, cultures were pelleted via centrifugation at 39,175 x g for 20 minutes at 4°C and stored at -80°C. Eventually this auto induction technique was used for MetNI and MSP expression with success and replaced the previous method of induction in Terrific Broth.

2.3 MetNI Transporter Purification

Wild-type and mutant MetNI proteins were purified using an ÄTKA Pure FPLC System (GE Healthcare) via affinity chromatography followed by size exclusion chromatography. All samples, lysates, and eluents were kept on ice or at 4°C unless otherwise noted. All MetNI constructs were purified identically except for the MetNI-FLAG fusion protein. The purification scheme was based on a previously described method [3] with slight variations. 15 g of MetNI cells were homogenized in MetNI buffer (50 mM TAPS pH 8.5, 250 mM NaCl, and 0.05% n-Dodecyl

β-D-maltoside (DDM, Anatrace). Additional DDM was added to 1.0% to solubilize membranes. 1.5 mg Deoxyribonuclease I (Sigma), 1.5 mg lysozyme (Sigma), and one protease inhibitor tablet (Roche) were added to the homogenate and was stirred for 20 minutes. The suspension was sonicated on ice using a flat tip sonicator with 30% bursts of 50 kHz for 45 seconds followed by 90 seconds of cooling for 4 cycles for a total of 3 minutes of sonication. The lysate was then stirred for 20 minutes and centrifuged at 48,254 x g for 20 minutes. The clarified supernatant was collected and 4 M imidazole (pH 8) was added to a final concentration of 25 mM. The lysate was injected onto three tandem 5 mL Ni-NTA HisTrap FF columns (GE Healthcare) equilibrated in MetNI buffer, washed with 60 mL of MetNI buffer containing 25 mM imidazole, followed by 75 mL of MetNI buffer containing 75 mM imidazole. The column was eluted with 15 mL of MetNI buffer containing a final concentration of 350 mM imidazole. Peak fractions were collected and loaded onto a HiPrep 26/10 Desalting column (GE Healthcare) equilibrated in MetNI buffer to remove imidazole. Peak fractions were collected, pooled (typically 10-12 mL total) and frozen in liquid nitrogen and stored at -80˚ C. The next day, the eluate was thawed, concentrated to 5 mL using an Amicon Ultra-15 Centricon with a 100,000 kD molecular weight cutoff (Millipore), filtered with a 0.2 µm filter, and injected onto a Superdex 200 pg 16/600 sizing column (GE Healthcare). Peak fractions (eluting at approximately 60 mL elution volume) were collected, pooled, and concentrated as before until the final protein concentration was approximately 15 mg/mL (extinction coefficient 83,000 $M^{-1} \times cm^{-1}$). Protein was then flash frozen with liquid nitrogen and stored at -80°C.

FLAG-tagged MetNI was purified in a similar manner using FLAG antibody affinity chromatography. The purification procedure was identical until the preparation of the clarified lysate; no imidazole was added. The supernatant was injected onto a XK 16 Column (GE Healthcare) packed with 15 mL of M2 anti-FLAG resin (Sigma) equilibrated with MetNI buffer. The column was washed with 100 mL of MetNI buffer, and then eluted with 20 mL 0.1 mg/mL 3xFLAG

peptide (Sigma) in MetNI buffer. For the latter, the flow was paused after 15 mL for 30 minutes to allow the FLAG peptide to reach binding equilibrium with the M2 anti-FLAG resin. This pause was necessary to ensure complete disassociation of the FLAG-tagged MetNI from the column. Peak fractions were collected, pooled (approximately 5 mL), flash frozen in liquid nitrogen and stored at -80°C. The next day, the eluate was thawed, filtered through a 0.2 µm filter, and injected onto a Superdex 200 pg 16/600 sizing column equilibrated with MetNI buffer. Peak fractions were collected, pooled, and concentrated to ~10 mg/mL, frozen with liquid nitrogen and stored at -80°C.

2.4 MetQ Purification

MetQ purifications were carried out as previously described [4]. The periplasmic extract of post-transcriptionally mature, signal peptide-cleaved MetQ was obtained by osmotic shock, which results in the lysis of only the outermost membrane of the cell. 10 g of cells were resuspended in 10 mL of 40% sucrose, 10 mM Tris-HCl pH 7.5, and 1 mM ethylenediaminetetraacetic acid (EDTA) and stirred for 30 minutes at room temperature. The cell suspension was then osmotically shocked with the addition of 500 mL of 4°C deionized H_2O and stirred for 20 minutes at 4°C. All subsequent steps were performed at 4°C. Stock solutions were added to a final concentration of 25 mM Tris pH 7.5, 150 mM NaCl, 17 mM imidazole, and 2 mM β-mercaptoethanol (BME) and centrifuged at 39,175 x g for 60 minutes to clarify the suspension. The supernatant was then injected onto three tandem 5 mL Ni-NTA HisTrap FF columns equilibrated with 25 mM Tris pH 7.5, 150 mM NaCl, and 2 mM BME (MetQ buffer) and washed with 150 mL of MetQ buffer containing 17 mM imidazole. The column was eluted with 15 mL of MetQ buffer containing 300 mM imidazole, peak fractions were collected and injected onto a HiPrep 26/10 desalting column equilibrated with MetQ buffer to remove imidazole. Peak fractions were collected (typically 10-12 mL) and frozen in liquid nitrogen and stored at -80°C. The eluate was thawed and concentrated to 5 mL using an Amicon Ultra-15 Centricon with a 10,000 kD molecular weight cutoff (Millipore), filtered and injected onto a Superdex 200 pg 16/600 sizing

column. Peak fractions (eluting at approximately 90 mL elution volume) were collected and concentrated until the protein concentration was approximately 30 mg/mL (extinction coefficient 2,040 $M^{-1} \times cm^{-1}$), frozen in liquid nitrogen and stored at -80°C.

The substrate-free purification was identical until the washing step; 150 mL of unfolding buffer (6M guanidine-HCl, 150 mM NaCl, 25 mM Tris pH 7.5, 2 mM BME) was flowed over the affinity immobilized MetQ to unfold the protein, then a 0-100% gradient of MetQ buffer for 90 minutes was flowed over the columns at a rate of 1 mL/min, with an additional 30 mL of 100% MetQ buffer to ensure proper refolding. The protein was then eluted, desalted, sized and concentrated using the aforementioned method to a concentration of 3.5 mg/mL, frozen in liquid nitrogen and stored at -80°C.

2.5 Membrane Scaffold Protein Purification

MSP1D1 and MSP1E3D1 purification were carried out identically to each other with minor exceptions. All samples, lysates, and eluents were kept on ice, or at 4°C unless otherwise noted. 15 g of MSP1D1 expressing BL21-Gold (DE3) cells were homogenized in 150 mL of MSP buffer (50 mM Tris pH 7.5, 100 mM NaCl) with 1 mM PMSF final. The suspension was sonicated using a flat tip sonicator with 30% bursts of 50 kHz for 45 seconds followed by 90 seconds of cooling for 4 cycles for a total of 3 minutes of sonication and centrifuged at 48,254 x g for 20 minutes. The clarified supernatant was injected onto a 5 mL Ni-NTA HisTrap FF column equilibrated with MSP buffer and washed with 45 mL MSP buffer containing 15 mM imidazole. The column was eluted with 15 mL of the MSP buffer containing 400 mM imidazole, peak fractions were collected and loaded onto a HiPrep 26/10 desalting column equilibrated with MSP buffer to remove imidazole. Peak fractions were collected and concentrated to approximately 10 mg/mL (extinction coefficient 21,430 $M^{-1} \times cm^{-1}$ for MSP1D1 and 29,910 $M^{-1} \times cm^{-1}$ for MSP1E3D1) using an Amicon

Ultra-15 Centricon with a 10,000 kD molecular weight cutoff for MSP1D1 and a 30,000 kD molecular weight cutoff for MSP1E3D1, frozen with liquid nitrogen and stored at -80°C.

2.6 General Conditions for Nanodisc Reconstitutions

Lipids were prepared previously by Janet Yang [5]. Briefly, phosphatidylcholine from chicken egg (Avanti) was added to *E. coli* Polar Lipid Extract (Avanti) at a ratio of 1:3 PC to lipids to give a final lipid profile of approximately 50% phosphatidylethanolamine (PE), 25% PC, 17% phosphatidylglycerol (PG) and 7% cardiolipin (CA) by mass with an average molecular weight of 791 daltons. The mixture was evaporated under a stream of argon, and the lipid film was gently dissolved in nanodisc buffer (50 mM TAPS pH 8.5, 250 mM NaCl) to 20 mg/mL and incubated with shaking at 120 rpm. Dissolved lipids were aliquoted and stored at -80°C.

For use in reconstitutions, varying amounts of DDM or cholate was added to the lipid mixture (as described in the results section) and was placed in a water bath and pulse sonicated in 5-sec pulses for 5 minutes before being returned to ice with other components. Amberlite XAD-2 adsorbent Bio-Beads (Sigma) were equilibrated in nanodisc buffer at room temperature. Subsequent steps were performed at 4°C. All components were added to a 2 mL Eppendorf tube in the order of lipid, buffer, MSP1, then and MetNI. Final concentrations of Tris, TAPS, and NaCl were slightly variable due to the addition of different volumes of each component. The mixture was placed on a nutating mixer overnight and then centrifuged at 16,000 x g for 10 minutes. The supernatant was filtered using a 0.2 µm centrifugal filter and injected onto a Superdex 200 Increase 10/300 GL sizing column equilibrated in nanodisc buffer. Peak fractions were collected and concentrated using an Amicon Ultra-15 Centricon with a 100,000 kD molecular weight cutoff to approximately 1.5 absorbance units at 280 nm. Samples not used immediately were frozen in liquid nitrogen and stored at -80ºC.

2.7 Native and SDS-PAGE

Denaturing sodium dodecyl sulfate polyacrylamide gel electrophoresis (SDS-PAGE), blue native PAGE (BN-PAGE) and non-denaturing clear native PAGE (CN-PAGE) were performed on purified proteins and nanodisc reconstitutions. For SDS-PAGE, 1 µg of purified protein was combined with gel loading buffer to a final concentration of 2% SDS, 10% glycerol, 10 mM EDTA, and 60 mM dithiolthreitol (DTT) and 0.02% bromophenol blue. Cell lysates, supernatants and column eluent samples were heated to 100ºC for 5 minutes, centrifuged at 16,000 x g for 5 minutes at 4ºC, then loaded onto Precast "Any kD" Mini Protean Gels (Bio-Rad) with 5 µL of Precision Plus Protein Ladder (Bio-Rad). Running buffer consisted of 25 mM Tris pH 8.3, 192 mM glycine, 0.1% SDS, and gels were electrophoresed at 50 mA, 200V for 30 minutes at room temperature. The gels were stained with 50 mL of a solution containing 40% methanol, 10% acetic acid and 0.25% Coomassie Blue R-250 for 30 minutes with rocking. Gels were then de-stained in 40% methanol and 10% acetic acid overnight and imaged the following day on a ChemiDoc imaging system (Bio-Rad).

BN-PAGE was performed with samples of varying protein amounts (typically 2-5 µg) in 12 µL of the respective purification or nanodisc buffer combined with 5% glycerol and 0.01% Ponceau S. Samples were kept on ice and loaded onto a 4-20% acrylamide 24-Well Criterion gel (Bio-Rad). The proteins β-amylase, alcohol dehydrogenase, and bovine serum albumin were always included as known molecular weight standards for BN-PAGE. The anode casket of the gel was submerged in a 4ºC buffer containing 50 mM Tricine,15 mM Bis-tris methane, pH 8.0 and 0.02% Coomassie Brilliant Blue G-250, while the cathode was submerged in a 4ºC buffer containing 50 mM Tricine pH 8 and 15 mM Bis-tris. The gel box was enveloped in ice to maintain a temperature near 4ºC and electrophoresed at 32 mA, 150V for 2 hours. The gels were fixed and de-stained overnight with the same de-staining solution used for SDS-PAGE and imaged the

following day. CN-PAGE was performed using the same method as BN-PAGE, however Coomassie Brilliant Blue G-250 was not added to the anode buffer of the cell.

2.8 SYPRO-Ruby Nanodisc Quantification

MetNI MSP1D1 nanodisc samples were diluted in 0.25 mg/mL increments in nanodisc buffer for quantification. The dilutions were made in the range of 0.5-2.5 mg/mL (extinction coefficient = 125,860 $M^{-1} \times cm^{-1}$). BSA samples were diluted to 0.5-1.5 mg/mL in increments of 0.25 mg/mL for a standard curve. Samples and gels were treated as per the SDS-PAGE protocol until staining. The gel was submerged in 100 mL of SYPRO Ruby Fixing Solution (Thermo Fisher) with rocking for 30 minutes. The fixing solution was then removed and 60 mL of SYPRO Ruby Staining Solution was added. The container was wrapped in foil and rocked overnight to remove unincorporated dye. The next morning, the gel was washed twice with 100 mL of SYPRO Ruby Wash Solution for 30 minutes each and then imaged with UV light on the ChemiDoc imaging system. The ChemiDoc software default fluorescence volume tool was used to generate a standard curve of mass to intensity via fluorescence densitometry. The standard curve was then used to calculate absolute mass of each band, and then used to calculate the mass ratio of all components of the nanodisc samples.

2.9 MetNI Nanodisc Complex-Immunoprecipitation

All of the following procedures were conducted 4ºC. 1.5 mL of Ni-NTA agarose beads was equilibrated in nanodisc buffer in a 15 mL conical tube. Approximately 1 mg of FLAG-MetNI MSP1D3E1 nanodiscs in 1 mL nanodisc buffer was added to the beads and gently rocked for 5 minutes. The beads were pelleted via centrifugation at 16,000 x g for 10 minutes, and the supernatant was collected. The beads were then washed three times by addition of 15 mL of nanodisc buffer, centrifugation, and removal of supernatant. The complex was eluted from the beads with 1 mL of nanodisc buffer containing 350 mM imidazole by mixing for 5 minutes. The

eluent was added to 2 mL of M2 anti-FLAG resin (Sigma) equilibrated in nanodisc buffer and mixed with gentle rocking for 5 minutes. The resin was pelleted via centrifugation at 16,000 x g for 10 minutes, and the supernatant collected. The resin was then washed as described above. The complex was eluted from the resin by adding 120 µg of 3xFLAG peptide in 600 µL of nanodisc buffer. All samples were immediately used for size exclusion chromatography and PAGE.

2.10 ATPase Activity Assays

Production of inorganic phosphate in solution was measured over time using an Enzchek Phosphate Assay Kit (Invitrogen) as published previously [5]. To convert the measured absorbance to concentration of inorganic phosphate, a phosphate standard curve was generated and fit using linear regression. The average slope from 4 standard curves was used for data analysis. Each detergent-based 100 µL reaction contained 60 mM Tris, pH 7.5, 5 mM TAPS, pH 8.5, 0.055% DDM, 55 mM NaCl, 200 µM MESG (2-amino-6-mercapto-7-methylpurine riboside), and 0.1 units of purine nucleoside phosphorylase. Each reaction contained 300 nM MetNI and varying equimolar amounts of $MgCl_2$ and ATP as indicated. For nanodisc-based assays, DDM was excluded from all mixtures. Reactions were started by adding the specified amount of MetNI or MetNI-containing nanodiscs and immediately measured on an EnVision 2103 Microplate Reader (PerkinElmer) at 22°C. Rates of inorganic phosphate generation were obtained by calculating the linear portion of the change in absorption at 360 nm as a function of time. All assays were performed in triplicate and the averaged values were analyzed using Prism software (GraphPad). Data were plotted as rate of absorbance change against ATP concentration and fit to the curve of the equation:

$$v = \frac{V_{max} \times [ATP]^n}{K_M^n + [ATP]^n}$$

where V_{max} is the maximum rate of ATP hydrolysis, K_M is the concentration of ATP at which the ATPase activity is half maximum, and n is the Hill coefficient. The K_M can be interpreted as a

measure of the protein affinity for ATP, and the Hill coefficient (*n*) is a measure of the cooperativity between the two ATP binding sites. The models and values were generated under the typical assumptions and limitations made for conformity to Michaelis-Menten enzymatic equations.

2.11 Fluorescence Labeling of MetQ

E. coli MetQ contains only one cysteine residue at position 23 in the amino acid sequence. Purified MetQ and N229A MetQ were labeled with fluorescein-5-maleimide (Thermo Fisher). 5 mg of purified MetQ was immobilized on 1 mL of Ni-NTA resin (Qiagen) and washed with 30 mL of a buffer containing 25 mM Tris pH 7.5, 150 mM NaCl, 10mM TCEP, pH 7.5. A solution of 10 mM fluorescein-5-maleimide in DMF was added to the slurry at a final concentration of 100 µM. The reaction was covered and gently mixed for 1 hour at 4°C before quenching with a final concentration of 80 mM BME. The resin was washed with 30 mL of MetQ buffer and eluted with 1 mL of MetQ buffer containing 300 mM imidazole. The eluent was then injected onto a HiTrap Desalting 5 mL column (GE Healthcare) equilibrated with MetQ buffer. Peak fractions were collected, frozen with liquid nitrogen and stored at -80°C.

The degree of labeling was calculated via absorption at 280 and 495 nm, with the molar extinction coefficient of MetQ at 280 nm ε = 20,400 $M^{-1} \times cm^{-1}$, and the fluorescein molar extinction coefficient at 495 nm ε' = 68,000 $M^{-1} \times cm^{-1}$. The concentration of protein was calculated using the following equations

$$[MetQ] = \frac{Abs_{280} - (Abs_{495} \times CF)}{\varepsilon} \qquad CF = \frac{Abs_{280}}{Abs_{495}}$$

where CF is the Correction Factor compensating for the absorbance of 495 nm light. This value was used to calculate the molar ratio of fluorophore to protein via the equation:

$$protein\ labeled\ \% = \frac{Abs_{495}}{\varepsilon' \times [MetQ]}$$

2.12 Fluorescence Anisotropy Binding Assay of the MetNIQ Complex

Fluorescence spectroscopy experiments were performed on a Horiba Jobin Yvon FluoroMax-4 spectrofluorometer using Jobin Yvon FluorEssence Software. Anisotropy and polarization measurements were made in the “L format” using the “Anisotropy vs Single Point” method with an excitation wavelength of 465 nm and emission wavelength of 535 nm for 10 trials, with a target standard error of the mean of 2% for each reading. For detergent-based assays, each 120 µL binding reaction contained 50 mM TAPS pH 8.5, 250 mM NaCl, 0.05% DDM,1 mM ATP, 1 mM EDTA, and 200 nM WT fluorescein-labeled MetQ or N229A MetQ. A variable amount of MetNI was titrated into each reaction and incubated at 22°C for 30 minutes before being transferred to a 10 mm path length quartz cuvette. Assays using MetNI reconstituted in nanodiscs were conducted in the above conditions without DDM. Data was collected and plotted using Prism software (Graphpad). The concentration of the protein:ligand complex was calculated as

$$[P \cdot L] = L_T \times \frac{A - A_f}{A_b - A_f}$$

where L_T is total MetQ concentration, $[P \cdot L]$ is MetNI : MetQ complex concentration, A is the observed anisotropy, A_f is the anisotropy of the free ligand and A_b is the anisotropy of completely bound ligand. The last two parameters were manually inserted based on preliminary curve fitting.

2.13 References

[1] Kadaba, N. et al. The high-affinity E. coli methionine ABC transporter: structure and allosteric regulation. *Science* **2008**, 321(5886), 250–253.

[2] Studier F. W. Protein production by auto-induction in high density shaking cultures. *Protein Expression and Purification* **2005**, 41(1), 207–234.

[3] Johnson, E.; Nguyen, P. T.; Yeates, T. O.; Rees, D. C. Inward-facing conformations of the MetNI methionine ABC transporter: Implications for the mechanism of transinhibition. *Protein Science : a Publication of the Protein Society* **2012**, 21(1), 84–96.

[4] Nguyen, P.; Li, Q. W.; Kadaba, N. S.; Lai, J. Y.; Yang, J. G.; Rees, D. C. The contribution of methionine to the stability of the Escherichia coli MetNIQ ABC transporter-substrate binding protein complex. *Biological Chemistry* **2015**, 396(9-10), 1127–1134.

[5] Yang, J. G.; Rees, D. C. The allosteric regulatory mechanism of the Escherichia coli MetNI methionine ATP binding cassette (ABC) transporter. *The Journal of Biological Chemistry* **2015**, 290(14), 9135–9140.

Chapter 3. Assembly and Purification of Reconstituted MetNI Nanodiscs

To aid in recalling the reaction components and nomenclature of the experiments performed in this thesis, the table below is provided as a reference. It is important to note that the theoretical molecular weight only accounts for protein mass.

Table 3.1 Table of Transporter, Nanodisc and Standard Molecular Weights.

Abbreviation	Description	Molecular weight
MSP1 monomer	Membrane scaffolding protein 1D1	24.5 kD
MSP1 nanodisc	Dimeric protein-lipid assembly formed by MSP1	49.0 kD
MSP3 monomer	Membrane scaffolding protein E3D1	32.6 kD
MSP3 nanodisc	Dimeric protein-lipid assembly formed by MSP3	65.2 kD
MetNI	MetNI transporter in detergent micelles	122 kD
MetNI-ND1	MetNI transporter embedded in a MSP1 nanodisc	171 kD
MetNI-ND3	MetNI transporter embedded in a MSP3 nanodisc	187 kD
$MalFGK_2$	Maltose transporter in detergent micelles	171 kD
$MalFGK_2$-ND1	Maltose transporter embedded in a MSP1 nanodisc	215 kD
1:3:40	6:18:240 µM ratio of transporter : MSP : lipid components	--
B-Amylase	Protein Standard from Sweet Potato	200 kD
Alc-D	Protein Standard from Yeast	150 kD
BSA	Protein Standard from Bovine	66 kD
MetQ	Methionine Substrate Binding Protein	30 kD

3.1 Initial Reconstitutions

The first round of experiments to reconstitute MetNI in nanodiscs were performed while visiting the laboratory of Franck Duong at the University of British Columbia. Purified recombinant MSP1D1 (hereafter referred to as MSP1) was kindly provided by the Duong Group, and MetNI transporter was brought from USF. In general, these experiments followed protocols established in the Duong Group [1]. A simplified schematic of the reconstitution procedure is depicted in Figure 3.1.

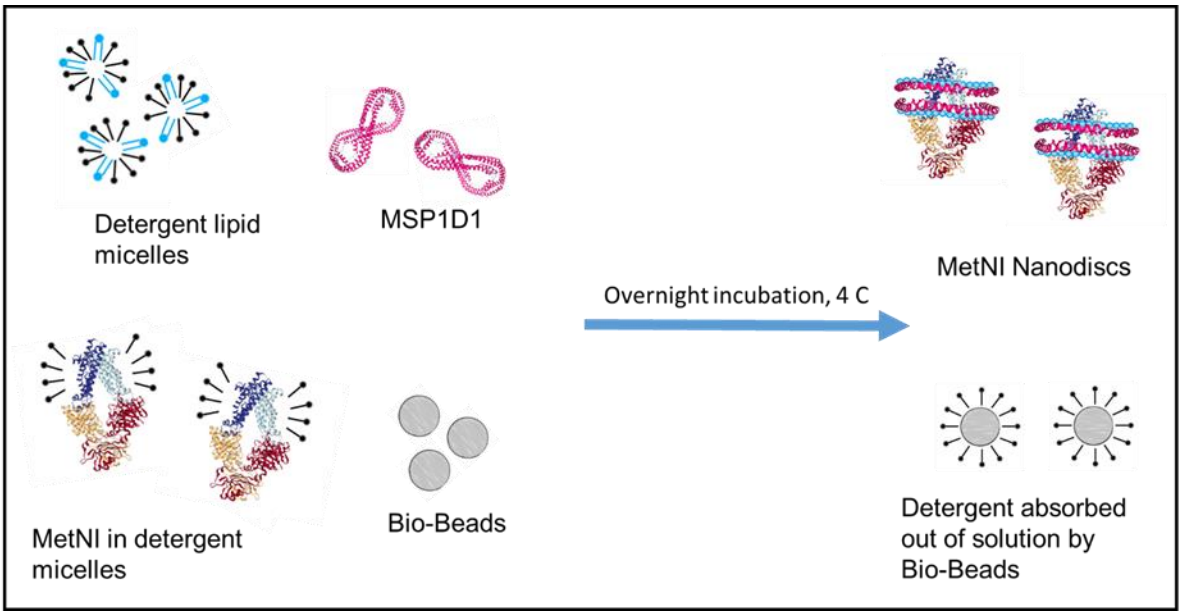

Figure 3.1. Schematic of the nanodisc reconstitution process using MetNI and MSP1D1. A lipid-detergent mixture is added to MSP1D1 and detergent-solubilized MetNI. After the addition of proteins and lipids, detergent is absorbed out of the mixture using Bio-Beads, which drives the aliphatic surfaces of the transporter to enter the more energetically favorable environment of the lipid disc.

These initial reconstitutions contained no added lipid. The rationale was that endogenous lipids remained associated with MSP1 during the purification process, and that a sufficient amount of lipid was present such that the transporter could be successfully reconstituted into the nanodiscs. Another reason for the initial exclusion of additional lipid was that a disproportionate amount of lipid tends to generate MSP1 aggregates [1,2]. For initial experiments, MetNI was diluted to a working stock of 2 mg/mL in MetNI buffer (50 mM TAPS pH 8.5, 250 mM NaCl, 0.05% DDM) and MSP1 diluted to a 7 mg/mL in TSG10 buffer (50 mM Tris pH 8.0, 100 mM NaCl, 10% glycerol) with a final detergent concentration of 0.1% DDM. The addition of different buffering solutions from each component altered the final concentration of each reconstitution listed, and thus the final concentrations of Tris, TAPS and NaCl varied slightly in these studies.

Overnight reconstitutions (300 µL) were performed in duplicate at MetNI : MSP1 : lipid ratios of 1:2:0, 1:3:0 and 1:4:0. The format of this molar ratio is imperative to understanding the ratios through this work. Unless otherwise noted, the standard concentration of MetNI used in a reconstitution was 6 µM, so a 1:2:0 ratio is a 6:12:0 µM mixture of MetNI to MSP1 to lipid. These molar ratios form the basis of the reconstitution work that described below, and was varied by scaling this base ratio as needed for the experimental conditions.

In these first experiments, 3 µg of reconstitution mixture was assessed via CN-PAGE (Figure 3.2). The amount of material was quantified via Bradford assay, and the gel composition was 4-12% acrylamide in 50 mM Tris, pH 8.8. The first lane in Figure 3.2 contains a positive control, the maltose transporter reconstituted in MSP1 nanodiscs. These maltose transporter nanodiscs, abbreviated as $MalFGK_2$-ND1, have a molecular weight of 215 kD [1]. Lanes 2-4 of the gel contain the experimental reconstitutions of MetNI in MSP1 nanodiscs. The calculated molecular weight of MetNI-containing MSP1 nanodiscs (hereafter referred to as MetNI-ND1) is 171 kD. The 1:3:0 and 1:4:0 reconstitutions contained a prominent single band as indicated by the arrow. Excess MSP1 monomer (24.5 kD) ran further down the gel, most visible in the

1:4:0 reconstitutions. The prominent species from the reconstitution experiments was smaller than MalFGK$_2$-ND1; however, given the relative position of MSP1 on the gel, the unknown band was much smaller than expected for MetNI-ND1.

We initially surmised that the faint middle band in the MalFGK$_2$-ND1 sample (lane 1) may be a good reference point to aid in analysis. Detergent-solubilized MalFGK$_2$ has a molecular weight of 171 kD, which is equal to the calculated molecular weight of MetNI-ND1. However, as seen in the gel, the faint middle band of the MalFGK$_2$-ND1 sample and the prominent band in the MetNI-ND1 reconstitutions do not align. These puzzling results were complicated further as the findings could not be reproduced in the Yang lab at USF, as discussed later in this chapter.

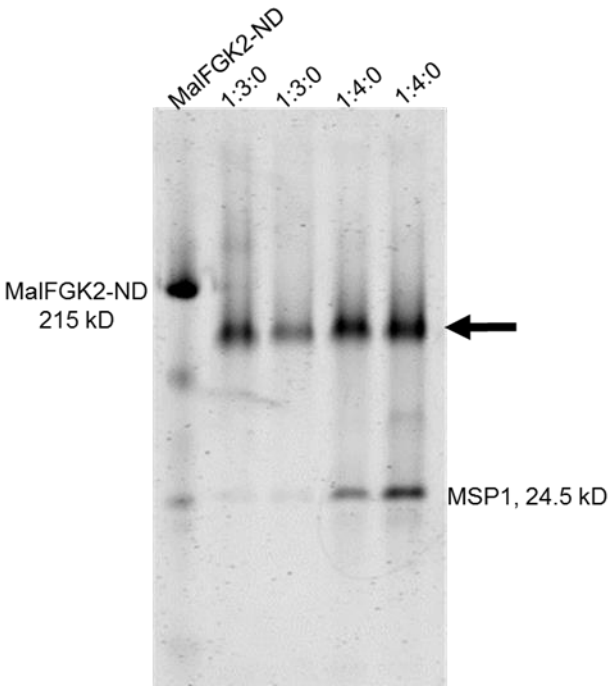

Figure 3.2. CN-PAGE of initial nanodisc reconstitutions at UBC. Reconstitutions of MetNI : MSP1 : lipid at the indicated molar ratios were incubated overnight with Bio-Beads and loaded onto a 4-12% polyacrylamide gel. MalFGK$_2$ -ND1 were included as a positive control. The most prominent band, indicated by the arrow, was smaller than expected for MetNI-ND1.

3.2 Purification of MSP1D1 and Yang Lab Reconstitutions

With a preliminary version of a MetNI reconstitution protocol in hand, all subsequent experiments were conducted at USF. MSP1 was expressed and purified in house. Reconstitutions at 1:2:0, 1:3:0, and 1:4:0 ratios were performed in triplicate and assessed via CN-PAGE, using a commercially available precast “Any kD” Mini Protean Gel (Bio-Rad) (Figure 3.3). Bovine serum albumin (BSA, 66 kD), alcohol dehydrogenase (150 kD), and β-amylase (200 kD) were combined in loading buffer and used as molecular weight markers. The alcohol dehydrogenase band was extremely faint, even at high concentrations, and was often excluded from subsequent CN-PAGE. BSA can run as both a monomer and a homodimer, the latter of which runs as a faint band at 132 kD on CN-PAGE.

As additional reference points, MetNI alone and MSP1 alone were included on the gel. Detergent-solubilized MetNI samples contained a high concentration of DDM detergent and thus did not run very far into the gel matrix. This limitation resulted in a large “U” shaped smear near the top (Figure 3.3, lane labeled “5 µg MetNI”). This observation is consistent with other studies of various DDM-solubilized materials, and the smear is most likely due to the impediment by the nonionic micelle. Purified MSP1 showed multiple bands (lane labeled “5 µg MSP1”), with the most prominent band believed to be empty nanodiscs, comprised of two MSP1 polypeptides and endogenous lipids, while MSP1 monomer (24.5 kD) ran further into the gel. Perplexingly, purified MSP1 also contained a larger species that was similar in size to that of the reconstitution samples (Figure 3.3, arrow).

At first glance these MetNI reconstitutions appeared significantly altered from previous experiments performed in the Duong Group (compare Figures 3.2 and 3.3). This discrepancy was potentially due to the switch from a homemade 4-12% polyacrylamide gel to the proprietary formulation of the Bio-Rad “Any kD” polyacrylamide gel used at USF. Upon further inspection, the

most prominent species in every reconstitution appeared considerably smaller than the 200 kD β-amylase standard, consistent with previous results from the Duong Group. Numerous additional experiments were conducted but modifications did not result in significant changes in products (data not shown).

These initial reconstitutions relied on CN-PAGE as the primary tool to assess for successful reconstitution. This technique, however, separates not only size but also by net charge and structure. These properties can affect the movement of particles through the gel matrix, which could lead to difficult interpretation of results. Thus, additional standards and analytical techniques were needed to determine the identity of the reconstitution products.

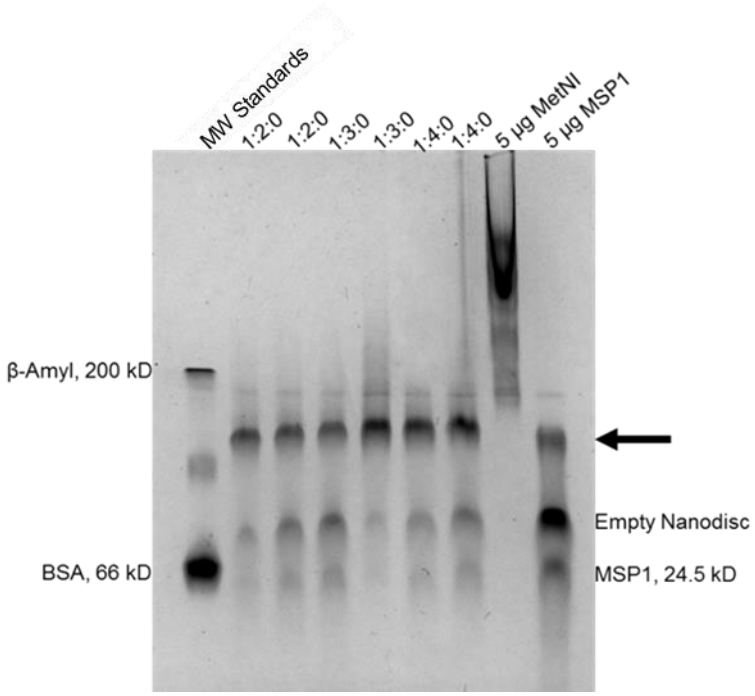

Figure 3.3. CN-PAGE of nanodisc reconstitutions at varying molar ratios of components at USF. Reconstitutions of MetNI : MSP1 : lipid at the indicated molar ratios were incubated overnight with Bio-Beads and loaded onto an Any kD Mini-PROTEAN TGX Precast Gel.

To further characterize our reconstitution samples, size exclusion chromatography was employed to approximate the size of products, where separations were performed at 1 mL/min to maintain consistent elution times and volumes and 1 mL fractions were collected during each run for comparison via gel. Under these conditions the recorded elution volumes for different species refer to the peak maximum as measured by absorbance at 280 nm.

For reference, detergent-solubilized MetNI was first injected onto a Superdex 200 10/300 GL sizing column (GE Healthcare) equilibrated in detergent-containing MetNI buffer (Figure 3.4A). The monodisperse peak containing detergent-solubilized MetNI eluted at 12.35 mL. Next, a reconstitution experiment using a 1:3:0 ratio of components was injected onto the same column equilibrated in TSG10 buffer (Figure 3.4B). Starting at the void volume of the column (8 mL), polydisperse protein complexes eluted over a 3 mL volume, followed by a predominant peak at 12.40 mL. The small peak at 16 mL was presumed to be excess monomeric MSP1.

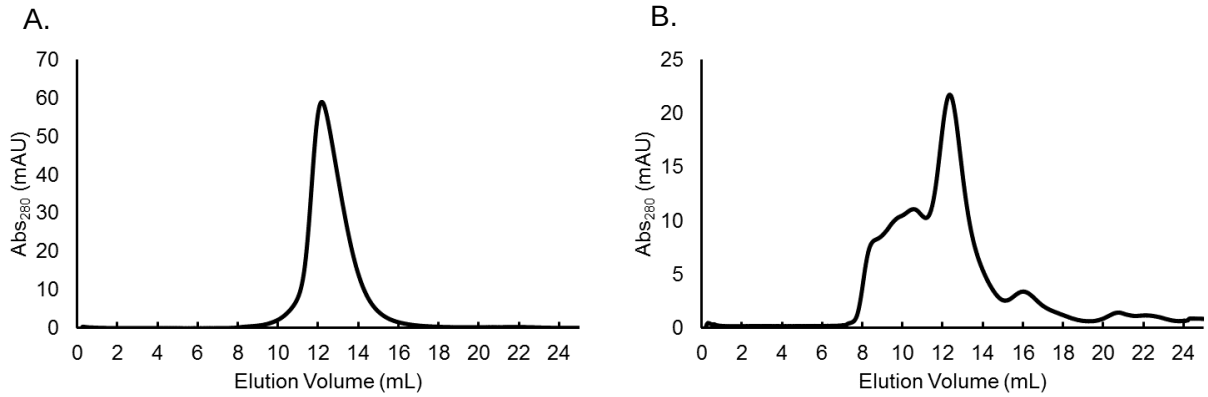

Figure 3.4. **Comparison of detergent-solubilized MetNI and MetNI nanodisc reconstitutions.** (A) Detergent-solubilized MetNI injected onto a Superdex 200 10/300 column equilibrated in detergent-containing buffer. (B) 1:3:0 reconstitution injected onto a Superdex 200 10/300 GL column in detergent-free buffer. Note that elution volume of the predominant peak in the reconstitution is very close to the elution volume for the monodisperse detergent-purified MetNI.

3.3 Nanodisc Reconstitution Troubleshooting

It was initially hypothesized that the reconstituted polydisperse eluent contained multiple nanodisc species and that the predominant peak was unincorporated MetNI transporter. In this case, since detergent-solubilized MetNI eluted at 12.35 mL (Figure 3.4A), the peak at 12.40 mL in the reconstitution was thought to be excess detergent-solubilized MetNI that had avoided aggregation in the reconstitution (Figure 3.4B). To test if the 12.40 mL reconstitution peak was unincorporated transporter, detergent-solubilized MetNI alone was subjected to the reconstitution protocol but without MSP1. This experiment included overnight incubation with Bio-Beads to remove detergent. If all detergent were successfully removed, we anticipated that the hydrophobic TMDs of MetNI would clump together into high molecular weight aggregates. A considerable amount of MetNI was used in this experiment (220 µg) to ensure that any remaining trace populations of micellar MetNI could be detected. These conditions only produced large aggregates as observed by SEC and native PAGE (data not shown). This data suggests that the detergent was sufficiently absorbed out of the mixture in our reconstitution protocol.

Another interpretation of the SEC results was that the 12.40 mL reconstitution peak was intact MetNI-ND1 (Figure 3.4B), however, this reasoning was inconsistent with the relative positions of the peaks from the two size exclusion experiments. MetNI alone is 122 kD and eluted at 12.35 mL and MetNI-ND1 has a predicted molecular weight of 171 kD, and thus the 12.40 mL reconstitution peak was interpreted to be too small to be intact MetNI nanodisc.

Given these inconclusive results, additional lipids were added to the reconstitutions as described by Bao et al [1]. The addition of *E. coli* polar lipids did not produce a discernible change in CN-PAGE results. Samples run on SEC showed a similar profile to that in Figure 3.4B; a primary peak eluted at 12.40 mL, and larger material did not resolve into individual peaks (data not shown). These reproducible, yet, unsatisfying findings, led us to re-evaluate the techniques

employed for our analysis. As for the movement of particles in native PAGE, SEC elution profiles can be variably affected by concentration, particle shape, solvent flow rate, buffer conditions, and the type of material used in the gel matrix. Thus, the limitations of both CN-PAGE and qualitative SEC necessitated a more analytical approach to accurately estimate the size of the reconstitution product.

For quantitative analysis of SEC chromatograms, a different size-exclusion column was employed. Our reconstitutions were then analyzed with a Superdex 200 10/300 GL column, which is used more frequently in preparative procedures rather than in analytical ones. To better utilize SEC as an analytical tool in the assessment of reconstitutions, an updated Superdex 200 10/300 pg Increase column was employed. This column offers increased resolution, which would potentially aid in the separation and identification of our reconstitution products. With this new column, it was first necessary to generate a calibration curve using standards of known mass. For this β-amylase (~200 kD), alcohol dehydrogenase (~150 kD), BSA (~66 kD) and purified MetQ (~30 kD) were individually injected onto the column. After calculating the partition coefficients (K_{av}) for each standard, the values were plotted against the log of the molecular weight of each protein (Figure 3.5). The data were best fit to the equation:

$$K_{av} = -0.121 ln(M_r) + 1.7417$$

where K_{av} is the partition coefficient of a species and M_r is the relative molecular weight of the species in units of Daltons. This standard curve was used to determine the relative molecular weight (M_r) of the different products of subsequent reconstitutions to approximate molecular weight (M_w).

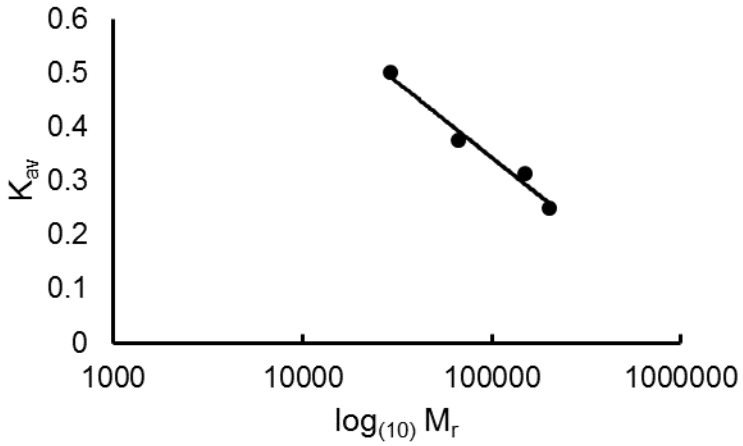

Figure 3.5. **Superdex 200 10/300 GL Increase calibration**. A calibration curve generated for Superdex 200 10/300 GL Increase column using the standards β-amylase, alcohol dehydrogenase, BSA and MetQ. The equation of the line was fit to the curve y = -0.121ln(x) + 1.7417 where the R^2 value = 0.978.

3.4 MSP1E3D1 Reconstitutions

Given the inconclusive results using the MSP1 scaffolding protein, we decided to use a longer membrane scaffold that could increase the yield of MetNI nanodiscs (see Chapter 1 for a discussion of different membrane scaffold proteins). MSP1E3D1 (hereafter referred to as MSP3) has a molecular weight of 32.6 kD and the calculated molecular weight of MetNI-containing MSP3 nanodiscs (hereafter referred to as MetNI-ND3) is 187 kD and our MetNI-ND3 reconstitutions were performed using procedures similar to those done with MSP1 but with changes to the buffer system. Specifically, glycerol was excluded from reconstitutions, and TSG10 buffer was replaced with nanodisc buffer (50 mM TAPS pH 8.5, 250 mM NaCl).

To more systematically analyze our experiments, we performed reconstitutions lacking either MetNI or MSP3 components as negative controls. Subsequently, all of the reconstitutions were injected separately onto a Superdex 200 10/300 GL Increase column equilibrated in nanodisc buffer at a flow-rate of 1 mL/min. These MetNI : MSP3 : lipid reconstitutions lacking MSP3 (1:0:40) always resulted in a single peak eluting at the void volume of 8 mL, as expected

(data not shown). These peaks were presumed to be aggregated MetNI that became insoluble after detergent removal. The second control included MSP3 but lacked MetNI. The MSP3-only 0:3:60 reconstitution generated three species, believed to be a small amount of aggregate, MSP3 nanodiscs without transporter, and MSP3 monomer (Figure 3.6A, orange trace). For ease of reading, the ratios of each component including the negative controls are provided in a table below.

Table 3.2. Table of Reconstitution Mixture Ratios

Abbreviation	Concentration of each component (MetNI : MSP : lipid)
1:3:40	6:18:240 µM
1:5:60	6:30:360 µM
1:0:40	6:0:240 µM (No MSP, negative control)
0:3:40	0:18:240 µM (No MetNI, negative control)

To determine the effects of lipid addition and MSP3 concentration on reconstitutions, we performed four experiments with varying amounts of nanodisc components. The final molar ratios for these reconstitutions were 1:3:40, 1:3:60, 1:5:40, and 1:5:60 and the results of the 1:3:60 reconstitution are discussed here. SEC resolved four distinct peaks (Figure 3.6B, blue trace). The peaks at 8 mL and 15 mL were observed in the earlier MSP3 alone reconstitution, and thus interpreted to be different MSP3 species without MetNI. The peaks at 10.60 and 12.10 mL were conjectured to be two different species MetNI-ND3.

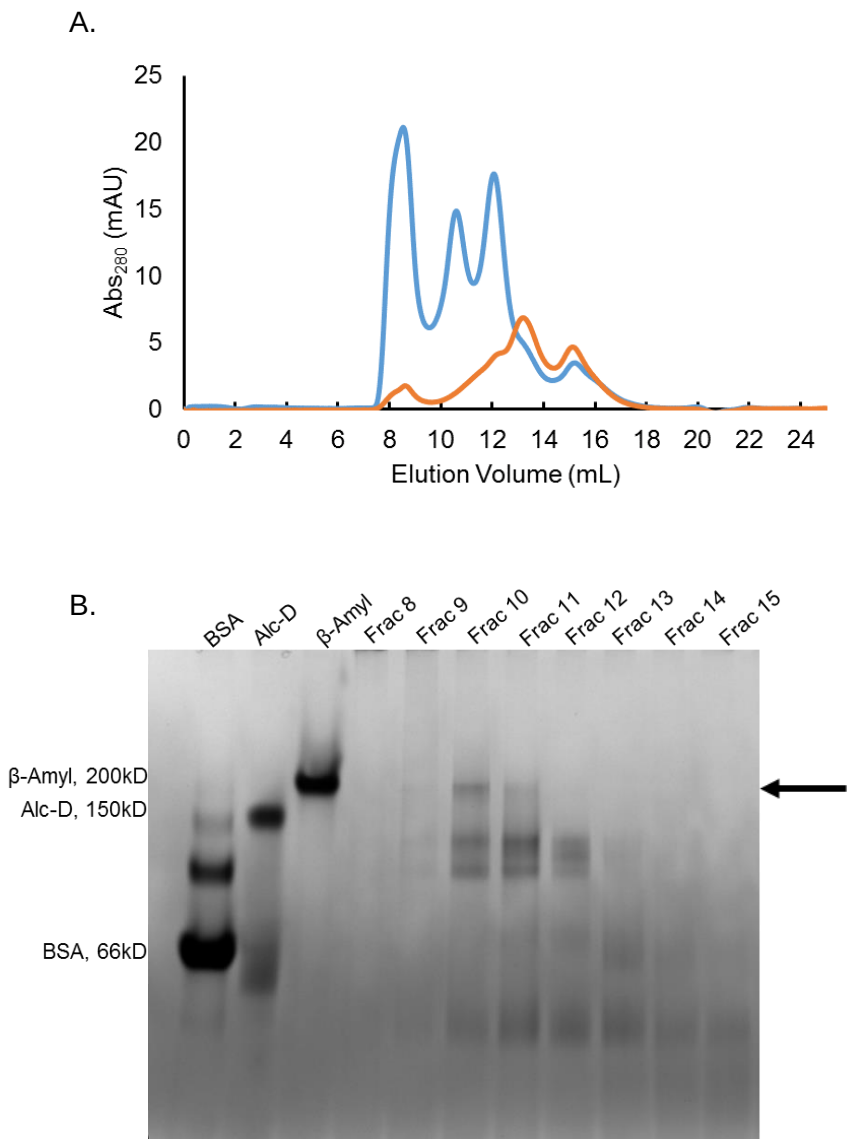

Figure 3.6. Reconstitutions using MetNI and MSP3. (A) SEC of a transporter free reconstitution (0:3:60 molar ratio of MetNI : MSP3 : lipid, shown orange) and a 1:3:60 reconstitution (shown blue). (B) BN-PAGE of corresponding SEC fractions from the 1:3:60 reconstitution loaded onto a 4-20% Criterion Tris-HCl gel. Aggregates in the void volume are not detected by gel (fraction 8), and a species of higher molecular weight, appropriate for MetNI-ND3, is present in fraction 10 (arrow).

The collected elution fractions were assessed on a different native PAGE system than was previously used. Specifically, BN-PAGE was performed using a 4-20% acrylamide 24-well Criterion gel (Bio-Rad) to give improved separation, resolution and sample detection revealing three distinct bands in the 10-12 mL fractions. The largest species in the 10 mL fraction appeared to be comparable in size to the 200 kD β-amylase protein standard and was considered to be a promising candidate for MetNI-ND3 (Figure 3.6B, arrow). However, based on the calibration curve for the column (Figure 3.5), the estimated size of the species in the 10 mL fraction is approximately 400 kD. Other products detected in the 11 and 12 mL fractions appeared smaller than the 150 kD alcohol dehydrogenase protein standard. Based on BN-PAGE alone, these species could be interpreted as MetNI that disassociated from the nanodisc or polypeptide components of the transporter that separated during electrophoresis.

Despite the conflicting interpretations of the 10.60 mL peak, we believed that the appearance of this band on BN-PAGE was evidence for the formation of MetNI-ND3. Conditions were explored to increase the desired product, including an increase in MSP3 from a 1:3:60 ratio to a 1:4:60 ratio. Additionally, the concentrations of each nanodisc component were increased in proportion to the original ratio. For ease of reading, a shorthand system was used to describe these scaled-up ratios, as seen in the table above.

Table 3.3. Table of Scaled Reconstitution Mixture Ratios

Abbreviation	**Concentration of each component (MetNI : MSP : lipid)**
1:3:60	6:18:360 µM
1:4:60 (2x)	12:48:720 µM
1:4:60 (3x)	18:72:1080 µM

Reconstitutions using 1:4:60 components were then analyzed by SEC. The change from a 1:3:60 ratio to a 1:4:60 ratio resulted in an increase in the relative size of the peaks at 10.60 and 12.10 mL compared to the aggregate peak at 8 mL (compare Figure 3.7 to Figure 3.6A). Furthermore, the increase in concentration of all components from 1:3:60 (1x) to 1:4:60 (2x) and 1:4:60 (3x) resulted in an increase of the absolute amount of all products, as detected by the increase in raw absorbance values.

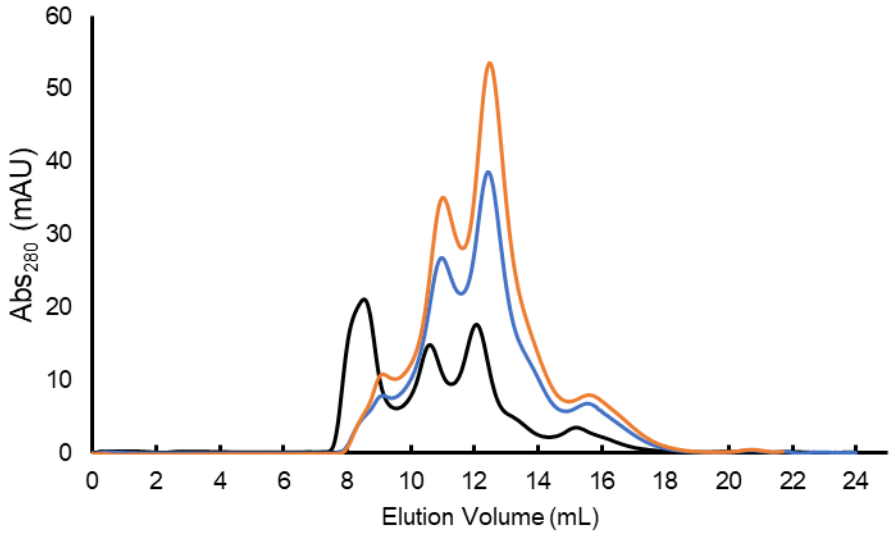

Figure 3.7. Increasing component concentrations for MSP3 reconstitutions. SEC chromatograms of a 1:4:60 MetNI : MSP3 : Lipid (2x) reconstitution (blue) and (3x) reconstitution (orange) show increased amounts of products in near identical stoichiometry. When compared to a 1:3:60 MetNI : MSP3 : Lipid reconstitution (black), the increased MSP results in a decrease of the largest aggregate peak (8 mL)

Ultimately, the experiments described thus far were inconclusive. Given the heterogeneity of the reconstitutions, inconsistencies in the molecular weights inferred by BN-PAGE and SEC, and the similarity between elution volumes for reconstitutions and for purified MetNI, it was therefore uncertain if intact MetNI-ND3 was being assembled. To test if MetNI and MSP3 were indeed creating a stable reconstituted nanodisc complex, a new experiment was devised, as described below.

3.5 Immunoprecipitation of the MetNI-ND3 Complex

To verify the successful formation of MetNI-ND3, a double affinity capture method was developed and executed. In this experiment, illustrated in Figure 3.8, the MetNI transporter contained a FLAG-tag (green squares), while MSP3 included a 10xHis-tag (blue squares) and 600 µl reconstitutions were assembled at a 1:4:60 (3x) molar ratio. Reconstitutions using these components gave rise to three possible species: (1) FLAG-tagged transporter, (2) His-tagged empty nanodiscs, (3) and doubly-tagged MetNI-ND3. To isolate the latter, two successive rounds of affinity chromatography were employed. This procedure is best described using a schematic with step-by-step instructions, found below in Figure 3.8.

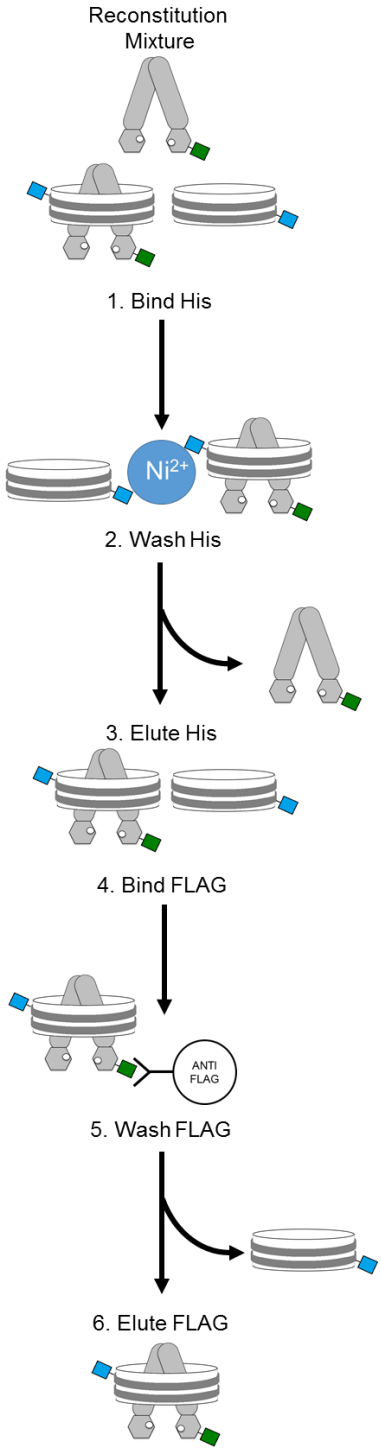

1. Reconstitutions were added to Ni-NTA resin, and species containing His-tagged MSP3 were immobilized on Ni-NTA resin.
2. Unbound FLAG-tagged MetNI that was not incorporated into nanodiscs was removed with washing.
3. Immobilized His-tagged MSP3 and MetNI-ND3 were eluted from the Ni-NTA resin.
4. The eluent was transferred to anti-FLAG resin and FLAG-tagged MetNI-ND3 was immobilized.
5. Unbound His-tagged MSP3 was removed with washing.
6. The remaining immobilized material was eluted by 3xFLAG peptide. The final product was assessed via BN- and SDS-PAGE.

Figure 3.8. Schematic of the co-immunoprecipitation procedure.

The final eluent from this co-immunoprecipitation (co-IP) was analyzed by BN-PAGE and SDS-PAGE (Figure 3.9). The gel-based results confirmed that MetNI-ND3 is present in the reconstitution. The 1:4:60 reconstitution resulted in one band on BN-PAGE (Figure 3.9A, last lane). This band was larger than the individual MetNI and MSP3 subunits and was not present in either of the negative control reconstitutions conducted in parallel (1:0:60 and 0:4:60). Surprisingly, MetNI-ND3 (187 kD) ran below alcohol dehydrogenase (150 kD). Furthermore, the majority of the initial reconstitution is the same size as the final elution sample (compare 1:4:60 6x lane with FLAG Elute lane). When analyzed on SDS-PAGE, the final elution consisted of potentially stoichiometric amounts of each component of the MetNI-ND3 complex (Figure 3.9B) and while the low concentration of the final eluent did not allow for subsequent analysis by SEC, the combined BN-PAGE and SDS-PAGE results confirmed that the reconstitution conditions were appropriate for forming a stable MetNI-ND3 complex.

The inconsistent BN-PAGE result can possibly be explained by two caveats of gel separations. Electrophoretic movement is proportional to the radius of the intact molecule and charge. This means that a more spherical molecule or complex can travel further through the decreasing width of the gel pores than a smaller but longer complex. Surface charge also significantly impacts movement, and the binding of negatively charged Coomassie dye to native structures and complexes can be less consistent compared to the well characterized binding and uniform charge to mass ratio of SDS to denatured polypeptides. We felt that the immunoprecipitation results demonstrated that a single complex on BN-PAGE with a small apparent size consisted of all three protein products on SDS-PAGE, and that the complex was successfully formed by nanodisc reconstitutions.

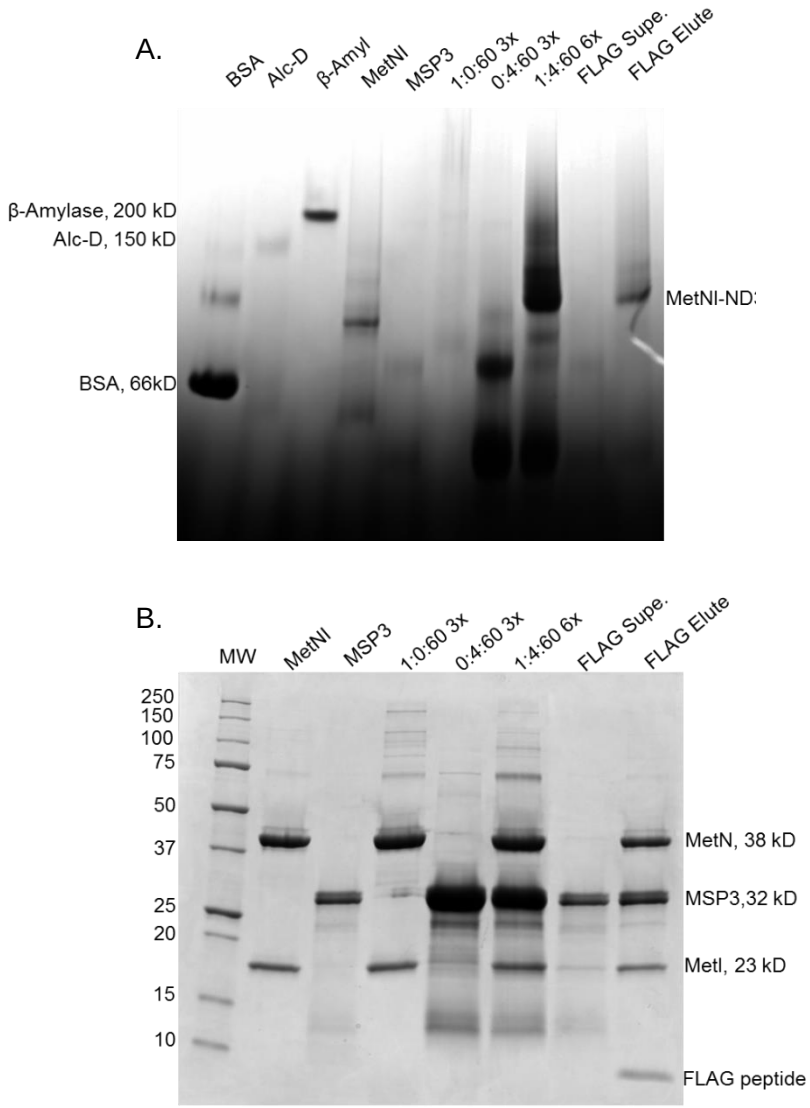

Figure 3.9. Co-immunoprecipitation of MetNI-ND3. (A) BN-PAGE of standards, individual nanodisc components, and reconstitutions. The co-IP eluent is loaded in the last lane. The single band indicates the presence of a single stable species. (B) SDS-PAGE of corresponding samples. The co-IP eluent, shown in the last lane, contains both MSP3 and MetNI, consistent with successful reconstitution of MetNI into nanodiscs.

3.6 Optimization of MetNI Nanodisc Formation

Confirmation of intact MetNI nanodiscs in MSP3 led us to re-evaluate our previous reconstitutions using MSP1. Initially, based on the calculated molecular weight of MSP1 and MetNI, the 10.5 mL eluted species appeared to be the target product when compared to standards on BN-PAGE (Figure 3.6B). However, using SEC, these complexes would be far larger (~400 kD) than the calculated molecular weight. Upon further review of the literature on the reconstitution of other ABC transporters with MSP1 and with MSP3, it was concluded that the 12.10 mL peak in MSP3 reconstitutions and the 12.40 mL peak in MSP1 reconstitutions were indeed successfully formed MetNI nanodiscs [1,3,4].

While the coimmunoprecipitation experiment resulted in very clean MetNI-ND3, the amount of starting material required for this process made it unrealistic for preparative purposes. Thus, we decided to go forward with MetNI nanodiscs purified using the previous SEC protocol. Despite the presence of contaminating bands in the peak fraction of our reconstitutions, we believed that we could produce enough MetNI nanodiscs by SEC to test for activity.

To determine which MSP construct (the 12.10 mL elution peak from MSP3 reconstitutions, or the 12.40 mL elution peak from MSP1 reconstitutions) yielded more target nanodisc product we performed a 1:6:60 (2x) reconstitution containing MSP1 alongside a 1:6:60 (2x) reconstitution containing MSP3 (Figure 3.10). In this experiment 1 mL SEC fractions were collected and assessed via BN-PAGE (Figures 3.10B and 3.10C).

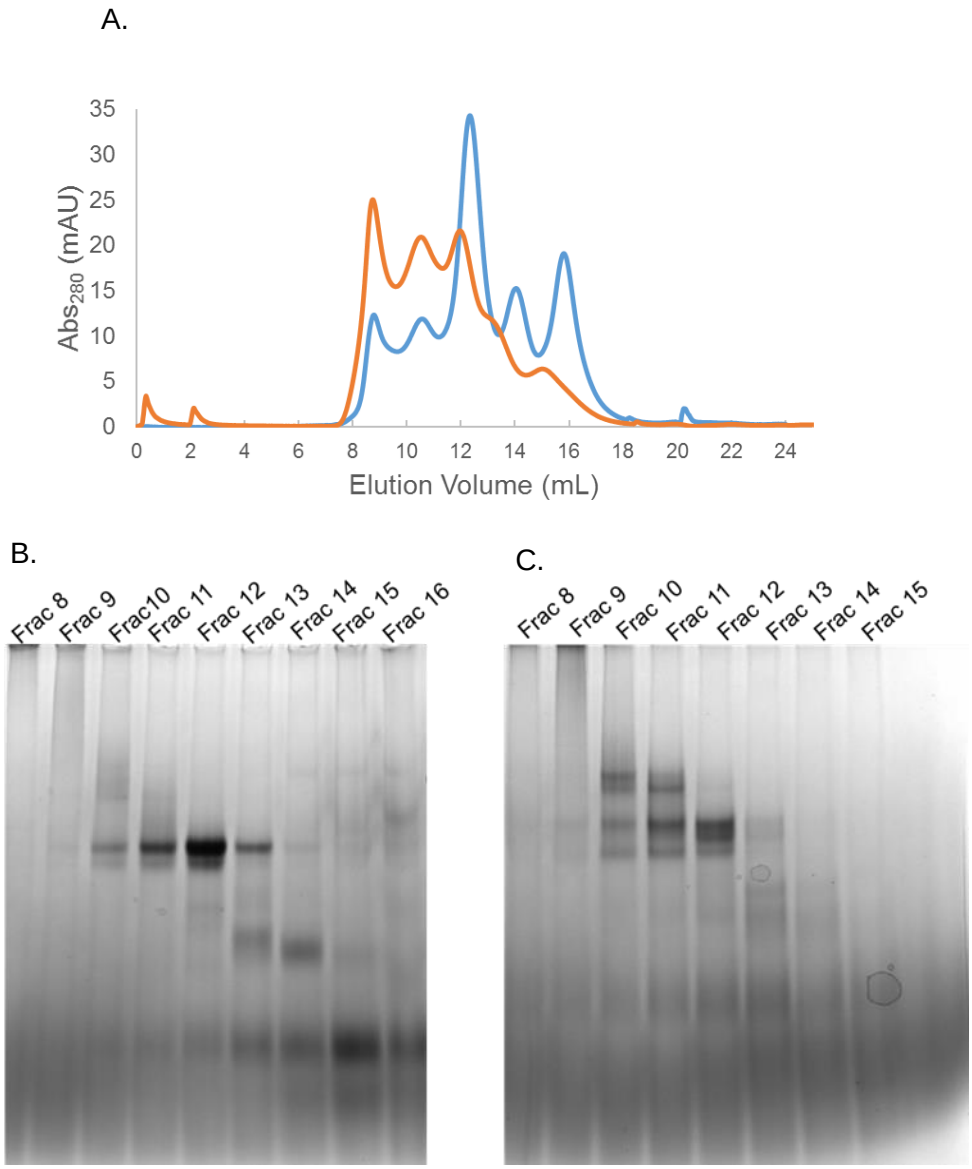

Figure 3.10. MSP1 is a better candidate than MSP3 for MetNI nanodisc reconstitutions. (A) SEC chromatogram of 1:6:60 (2x) reconstitutions using either MSP1 (blue) or MSP3 (orange). The MSP1 reconstitution generated more MetNI nanodiscs (12.40 mL peak) than the MSP3 reconstitution (~12.10 mL peak). (B) BN-PAGE of the corresponding elution fractions for the MSP1 reconstitution, showing enriched MetNI-ND1 in the 12 mL fraction. (C) BN-PAGE of fractionated MSP3 reconstitution with multiple contaminating larger products.

The results of this MSP1 versus MSP3 reconstitution comparison helped us determine the appropriate MSP for subsequent reconstitutions. Specifically, the MSP1 reconstitution was significantly enriched for the target product at 12.40 mL elution volume (Figure 3.10A, blue). As seen on the chromatograms, there was less of the contaminating species at 8.0 and 10.5 mL elution volumes, but there also remained excess empty nanodisc (14 mL) and monomeric MSP1 (16 mL). These results were confirmed by BN-PAGE (Figure 3.10B), with a significantly enriched band in fraction 12 of the MSP1 reconstitution. This target species contained a minor amount of a contaminating lower band that could not be resolved by SEC. The nature of this band was likely either disassociated of MetNI-ND1 or disassociated MetNI subunits (MetN or MetI alone). In contrast, the MSP3 reconstitution contained several products which were difficult to resolve by SEC (Figure 3.10A, orange). When examined by BN-PAGE, five distinct bands were detected in multiple fractions (Figure 3.10C). The extremely large complexes in the MSP3 reconstitutions ran as doublet bands in the 10 mL fraction, followed by a triplet of bands in the 12 mL elution fraction.

Overall, the MSP1 reconstitution generated greater amounts of MetNI nanodiscs with less aggregation and oversized complexes, as detected on both SEC and BN-PAGE. MSP1 was therefore chosen for subsequent reconstitution optimizations and scaling up.

3.7 MSP1 Reconstitution with Sodium Cholate

Further reconstitutions were also carried out using less MSP1 and lipid in an attempt to drive the assembly of more MetNI-ND1 and less empty disc and aggregates. A 1:4:40 (2x) reconstitution was assessed on SEC and BN-PAGE (Figure 3.11). The increased concentration of MetNI in the reconstitution appeared to drive more formation of the undesirable 10.5 mL eluting peak without increasing the amount of MetNI-ND1 at 12.10 mL (compare Figure 3.10A and Figure 3.11A). Additionally, the amount of empty nanodisc and MSP1 monomer contaminants in this reconstitution remained the same as previously found, despite the change in transporter and lipid

concentration. In summary, the 1:4:40 (2x) reconstitutions did not produce more MetNI-ND1 in comparison to the 1:6:60 (2x) conditions.

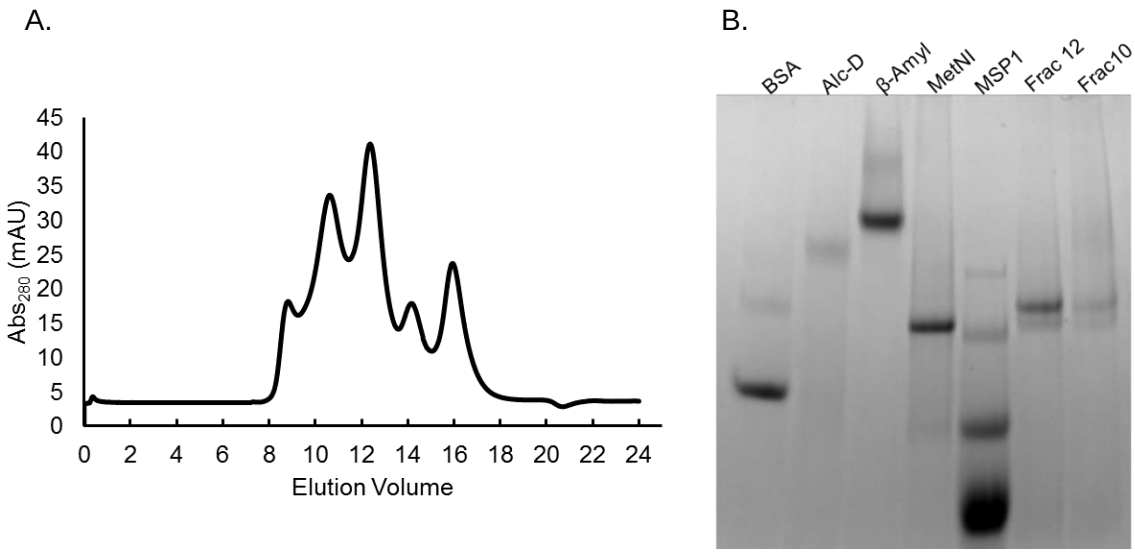

Figure 3.11. Larger scale MSP1 reconstitutions. (A) SEC chromatogram of a 1:4:40 (2x) reconstitution. Aggregates and large complexes (8.00 and 10.50 mL peaks) and MSP1 subunits (14 and 16 mL peaks) were still in abundance relative to the increase in product at 12.10 mL. (B) A BN-PAGE gel of the 10 and 12 mL SEC fractions. The 10 mL fraction contains higher molecular weight species above MetNI-ND1, and the 12 mL fraction includes a faint band below MetNI-ND1.

As previously observed in Figure 3.10B, both the main peak at 12.10 mL and the secondary peak at 10.50 mL contain a co-eluting double band (Figure 3.11B, fraction 12 and fraction 10 lanes). This contaminating band was assumed to be aggregated protein components in association with intact MetNI-ND1. Another notable development was that detergent-solubilized MetNI migrated as a single resolvable band on native PAGE if the detergent concentration was adequately lowered (Figure 3.11B, MetNI lane). This finding indicated how the transporter appears on native PAGE and was a useful negative control for further experiments.

Despite our attempts to increase the yield of MSP1 reconstitutions, the yield of MetNI-ND1 remained very low even after using non-trivial amounts of MetNI transporter per reconstitution. Reconstitutions that consumed 600 µg of MetNI reproducibly yielded only 60 µg of MetNI-ND1. To increase the yield the reconstitutions were then screened with the addition of sodium cholate to the lipid solution. Sodium cholate is a detergent that is often used in reconstitutions when the ideal amount of lipid is difficult to determine [2]. Although there were concerns regarding the effect of cholate on the physical structure of MetNI, a 1:3:60 (2x) reconstitution was performed with 3 mM cholate in place of additional DDM. A standard 1:3:60 (2x) reconstitution without cholate was prepared in parallel, as well as 1:3:40 (2x) and 1:3:90 (2x) cholate-free reconstitutions. The samples were then injected onto an SEC column and assessed via BN-PAGE (Figure 3.12).

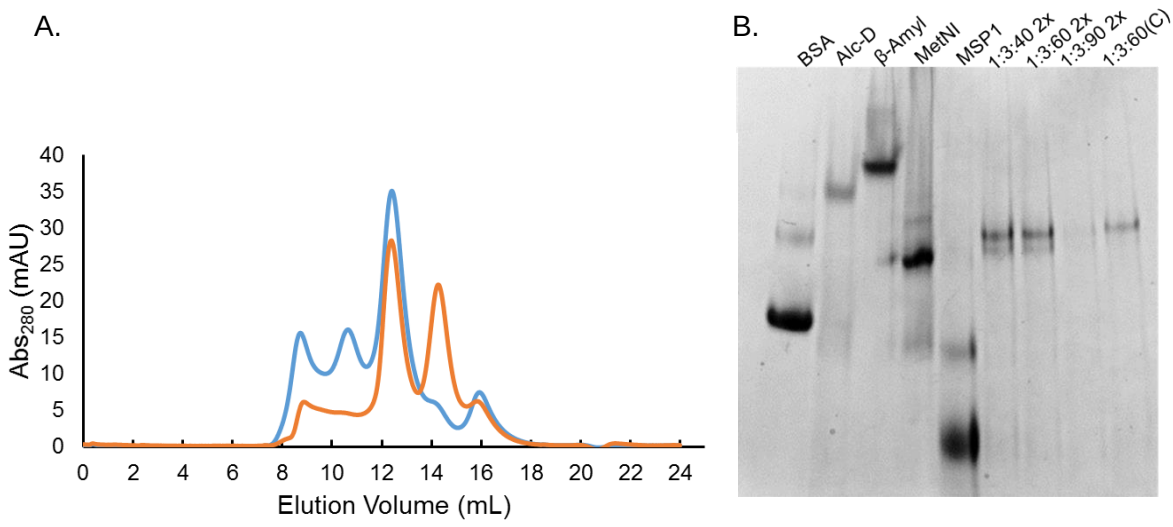

Figure 3.12. Sodium cholate disrupts formation of large undesirable MetNI reconstitution products. (A) SEC chromatogram of a 1:3:60 (2x) reconstitution with (orange) and without (blue) 3 mM sodium cholate. As a result of cholate addition, the peaks containing aggregates (8.00 and 10.50 mL elution volumes) were reduced but the corresponding empty nanodisc peak (14.00 mL) increased. (B) BN-PAGE of the 12 mL fraction from multiple reconstitutions**.** The addition of cholate (last lane) diminished the smaller doublet band seen in other MSP1 reconstitutions.

The addition of cholate had a distinct effect on the reconstitution products. Notably, all of the relative amounts of all species changed with the exception of MetNI-ND1 (compare orange and blue traces in Figure 3.12A). In addition, the amounts of aggregates and large complexes in the cholate-containing reconstitution were greatly reduced in comparison to the cholate-free reconstitution, but the amount of empty disc increased (Figure 3.12A; 8.0, 10.5 mL, and 14.5 mL elution peaks, respectively). The cholate-containing reconstitution also yielded slightly less MetNI-ND1 and more empty MSP1 nanodiscs, a tradeoff for the decrease in aggregate material. Additionally, when the 12 mL elution fraction from the cholate-containing reconstitution was analyzed by BN-PAGE, the doublet band present in previous MetNI-ND1 samples was absent (Figure 3.12B, last lane). This led us to the conclusion that the cholate was responsible for the disappearance of this smaller contaminant. Further screening of cholate reconstitutions allowed us to determine that half the previous cholate concentration, 1.5 mM final concentration, was ideal for the reconstitution of MetNI into MSP1, as was recommended in the literature [2,5].

3.8 Scale Up of MetNI-ND1 and MetNI N295A-ND1 Reconstitutions

We performed large-scale reconstitutions to generate enough MetNI-ND1 to begin characterizing its ATPase activity. The components included cholate, MSP1, lipids, and either wild-type MetNI or N295A MetNI (see Chapter 1 for a description of this mutant). Our 1:3:60 (3x) reconstitutions contained 1.5 mM sodium cholate at a total volume of 1 mL and the reconstitutions were purified by SEC and collected in 0.25 mL fractions to separate MetNI-ND1 (12.10 mL) from empty nanodisc (14.50 mL) (Figure 3.13). Unfortunately, separation of the two peaks was difficult, particularly for the MetNI N295A reconstitution (Figure 3.13B). The two peak fractions were pooled and concentrated to a final Abs_{280} value of 6.0 (wild-type MetNI) and 4.8 (N295A MetNI). The extinction coefficient of the nanodisc was calculated to be 125,860 $M^{-1} \times cm^{-1}$, giving an estimated concentration of 47 µM and 38 µM for wild-type MetNI-ND1 and N295A MetNI-ND1, respectively. The concentrations of both nanodiscs were verified via densitometry studies using

SDS-PAGE (data not shown). This concentration was deemed to be sufficient for functional studies.

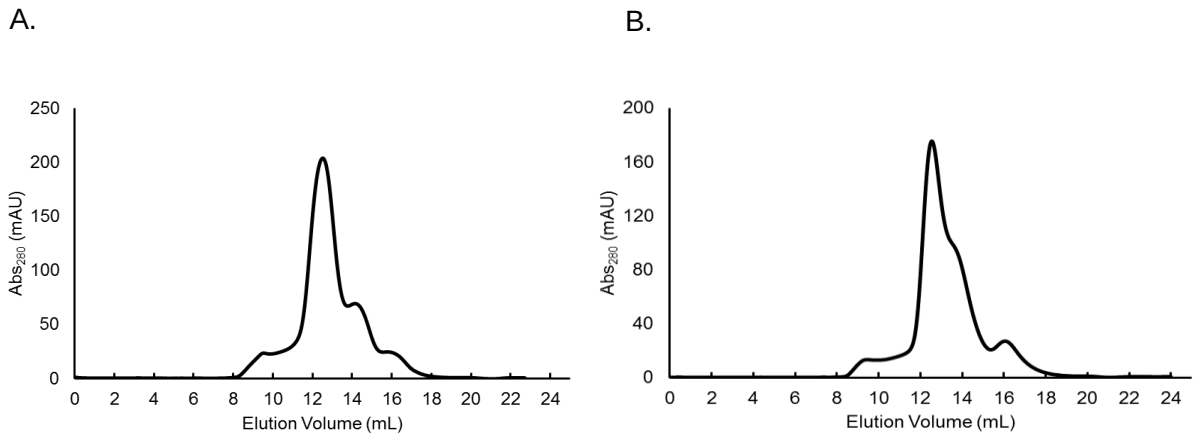

Figure 3.13. Size exclusion chromatography of high concentration reconstitutions of MetNI-ND1 and MetNI N295A-ND1. (A) SEC chromatogram of a 1:3:60 (9x) wild-type MetNI reconstitution containing 1.5 mM sodium cholate. (B) SEC chromatogram of a 1:3:60 (9x) N295A MetNI reconstitution containing 1.5 mM sodium cholate.

3.9 Initial Kinetic Characterization of MetNI Nanodiscs

The ATPase activity of MetNI-ND1 was compared to that of detergent-solubilized MetNI to examine the effect of a lipidic environment on MetNI function. As expected, detergent-solubilized wild-type MetNI hydrolyzed ATP in the absence of L-methionine (Figure 3.14A). We then fit our data to a modified Michaelis-Menten model that includes the Hill coefficient to account for cooperativity between two ATP sites. The best-fit kinetic parameters are as follows: $K_{M(ATP)}$ = 670 ± 50 µM, k_{cat} = 20 ± 2 min^{-1}, and the Hill coefficient (n) = 1.5 ± 0.2. The Hill coefficient greater than 1 suggests positive cooperativity between the ATPase sites, consistent with findings previously seen with MetNI [7-10]. MetNI-ND1 was able to hydrolyze ATP in the absence of the substrate (Figure 3.14A), which is similar to detergent-solubilized MetNI. The data were fit to a

model that yielded the following kinetic parameters: $K_{M(ATP)}$ = 1.2 ± 0.1 mM, k_{cat} = 32 ± 2 min^{-1}, and the Hill coefficient (n) = 1.1 ± 0.2. The latter result is surprising; the Hill coefficient suggests that cooperativity between the two ATPase sites is lost when MetNI is in a lipidic environment. Further experimentation will be necessary to substantiate this finding. More notably, while the $K_{M(ATP)}$ of MetNI-ND1 was higher than the K_M of detergent-solubilized MetNI, the k_{cat} also increased. These results are at odds with the hypothesis that the futile cycling of the ATPase may be caused by structural deformations of the enzyme caused by detergent micelles.

Next, we measured the ATPase activity of the detergent-solubilized N295A mutant in the absence of substrate (Figure 3.14B). As expected, the kinetic parameters were similar to that of detergent-solubilized wild-type MetNI with a K_M of 450 ± 30 µM, k_{cat} of 28 ± 2 min^{-1}, and a Hill coefficient of 1.5 ± 0.1, while the N295A MetNI-ND1 rates did not fit to an allosteric sigmoidal curve using the modified Michaelis-Menten model. This suggests that there may have been problems with the specific preparation of N295A MetNI-ND1, and thus this experiment merits further trials. Overall, these early functional studies are intriguing, and we presume future assays will reveal critical insights into the effect of lipids on MetNI function.

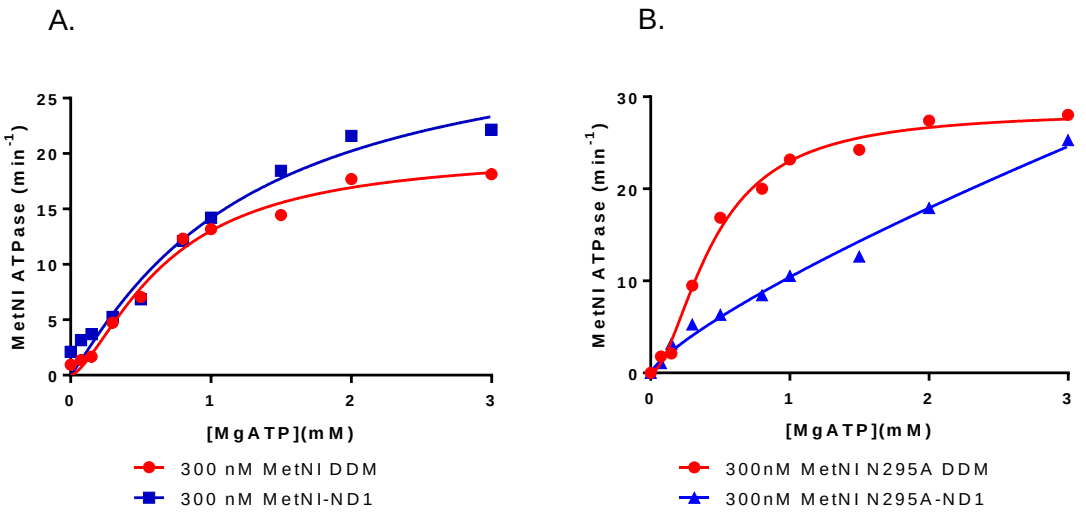

Figure 3.14. **MetNI-ND1 has similar ATPase activity to detergent-solubilized MetNI.** (A) The ATPase activity of detergent-solubilized wild-type MetNI (red) is compared to the activity of wild-type MetNI-ND1 (blue). (B) The ATPase activity of detergent-solubilized N295A MetNI (red) is compared to the activity MetNI N295A-ND1 (blue). Model convergence was not reached when fitting the MetNI N295A-ND1 ATPase activity.

Table 3.4 Table of Transporter Kinetic Values

Solubilized Transporter	$K_{M(ATP)}$	k_{cat} (min^{-1})	***n* (Hill Coefficient)**
MetNI (DDM)*	330 ± 20 µM	17 ± 1	1.7 ± 0.1
MetNI (DDM)	670 ± 50 µM	20 ± 2	1.5 ± 0.2
MetNI-ND1	1.2 ± 0.1 mM	32 ± 2	1.1 ± 0.2
MetNI N295A (DDM)	450 ± 30 µM	28 ± 2	1.5 ± 0.1
MetNI N295A-ND1	N/A	N/A	N/A

*Uninhibited MetNI ATPase activity as previously reported [7].

3.10 Fluorescence Anisotropy Assay for MetNIQ Complex Formation

Previous studies show that the formation of the MetNIQ complex requires an ATP-bound state of the MetNI transporter and the apo-form of the periplasmic substrate-binding protein MetQ [6]. This unexpected result represented a significant departure from the widely accepted models of transport. We hypothesize that this finding may be a consequence of using detergent-solubilized MetNI in binding measurements. To determine if the binding affinity of MetNI for MetQ is altered when embedded in a lipidic nanodisc, we developed a fluorescent anisotropy to measure dissociation constants. Specifically, fluorescein-labeled apo-MetQ was titrated with varying amounts of either detergent-solubilized MetNI or MetNI-ND1, with ATP and EDTA included to mimic the ATP-bound nucleotide state.

As seen in Figure 3.15, the fluorescence anisotropy of an apo-MetQ increased as a function increasing detergent-solubilized MetNI. These initial results were promising; however the assay could not be saturated to yield a complete binding isotherm. In addition, assays using MetNI-ND1 were inconclusive in these initial trials. One major limitation of these experiments was the 30-minute incubation period at 22ºC used to ensure binding equilibrium, which led to the aggregation of high concentration protein. Additionally, the anisotropy was often variable based on inconsistent labeling of MetQ. Despite these difficulties, with further optimization, anisotropy experiments with fluorescently-labeled MetQ may be a viable option to compare the dissociation constant of the MetNIQ complex in detergent versus in nanodiscs.

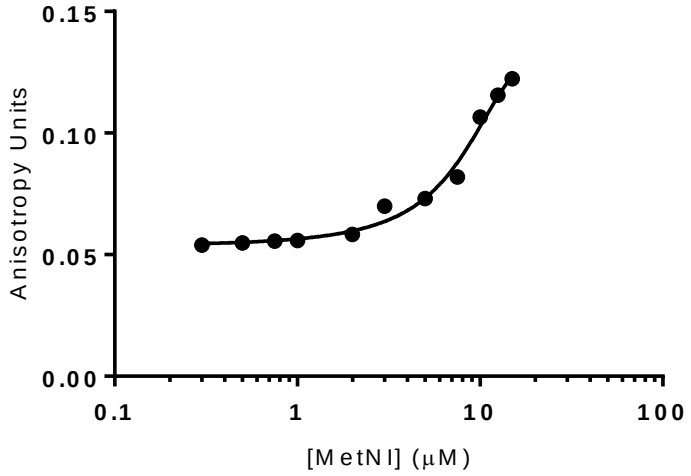

Figure 3.15. Fluorescence anisotropy of labeled MetQ increases with MetNI concentration. An apo-form of MetQ was titrated with increasing amounts of detergent-solubilized MetNI in the presence of ATP·EDTA. The assay did not reach saturation, and thus a disassociation constant was not calculated.

3.11 References

[1] Bao, H.; Duong, F.; Chan, C. S. A Step-by-step Method for the Reconstitution of an ABC Transporter into Nanodisc Lipid Particles. *Journal of Visualized Experiments* **2012**, 10.3791/3910.

[2] Bayburt, T.; Sligar, S.; Membrane protein assembly into Nanodiscs. *FEBS Letters*, **2010**, 584(9), 1721–1727.

[3] Korkhov, V.; Mireku, S.; Veprintsev, D. et al. Structure of AMP-PNP–bound BtuCD and mechanism of ATP-powered vitamin B12 transport by BtuCD–F. *Nature Structural and Molecular Biology* **2014**, 21, 1097–1099.

[4] Alvarez, F.; Joan D.; Orelle, C.; Davidson, A. Functional reconstitution of an ABC transporter in nanodiscs for use in electron paramagnetic resonance spectroscopy. *Journal of the American Chemical Society* **2010**, 10.1021/ja104047c.

[5] Denisov, I.; Sligar, S. G. Nanodiscs for structural and functional studies of membrane proteins. *Nature Structural and Molecular Biology* **2016,** 23, 6, pp. 481-486.

[6] Nguyen, P.; Li, Q. W.; Kadaba, N. S.; Lai, J. Y.; Yang, J. G.; Rees, D. C. The contribution of methionine to the stability of the Escherichia coli MetNIQ ABC transporter-substrate binding protein complex. *Biological Chemistry* **2015**, 396(9-10), 1127–1134.

[7] Yang, J. G.; Rees, D. C. The allosteric regulatory mechanism of the Escherichia coli MetNI methionine ATP binding cassette (ABC) transporter. *The Journal of Biological Chemistry* **2015**, 290(14), 9135–9140.

[8] Davidson A.; Laghaeian S.; Mannering DE. The maltose transport system of Escherichia coli displays positive cooperativity in ATP hydrolysis. *The Journal of Biological Chemistry* **1996**, 271:4858–4863

[9] Korkhov, V.; M.; Mireku, S. A.; Locher, K. P. Structure of AMP-PNP-bound vitamin B12 transporter BtuCD-F. *Nature* **2012,** 490(7420), 367–372.

[10] Tal, N.; Ovcharenko, E.; Lewinson, O. A single intact ATPase site of the ABC transporter BtuCD drives 5% transport activity yet supports full in vivo vitamin B12 utilization. *Proceedings of the National Academy of Sciences of the United States of America* **2013** 110(14), 5434–5439.

Chapter 4. Concluding Remarks and Future Work

4.1 Summary of Major Accomplishments

Ultimately, MetNI was successfully reconstituted into MSP1 and MSP3 nanodiscs and the first portion of this project was focused on verifying the identity of these reconstitution products. Once we obtained definitive evidence of MetNI nanodisc formation, we focused on increasing nanodisc yield. After successive rounds of optimization, we were able to successfully scale up reconstitutions to produce enough reconstituted MetNI nanodiscs for functional studies. Lastly, our preliminary functional assays provide a foundation for future examinations of MetNI transport.

4.2 Techniques for the Analysis of Reconstitution Products

The most challenging portion of this project was the verification of MetNI nanodisc formation. Existing literature claimed that the process was highly efficient and simple in comparison to alternative lipid environments like liposome reconstitutions [1]. In our hands, however, numerous experiments with different protein components were required before the product was clearly identified. In retrospect, some experiments could have been designed more systematically, but also the inherent limitations of the experimental techniques made the complexities we encountered unavoidable. Below is a discussion of the limitations of each technique and suggestions for future analysis.

Native PAGE is a common biochemical technique to study multi-component protein complexes. Unfortunately, there is not a universal native PAGE formulation that is ideal for all proteins. Through multiple attempts to visualize reconstitution products, we found that nanodisc products are particularly sensitive to changes in gradient gel formulation and electrophoresis conditions. Membrane protein complexes are commonly analyzed using CN-PAGE, as the gentler conditions retain the native state of these labile assemblies [2]. However, interpretation of CN-PAGE is complicated since the migration distance depends on intrinsic charge, shape, and mass.

In contrast, BN-PAGE eliminates the dependence on the intrinsic charge of the protein. In this technique, the binding of Coomassie dye coats the protein with negative charges while retaining the native protein state. For more delicate samples, however, BN-PAGE can often disrupt protein complex stability. In our hands, BN-PAGE proved to be the most reliable technique for high-resolution separation of nanodisc reconstitutions.

Size exclusion chromatography is a valuable tool to separate protein mixtures in solution. The separation and resolution provided by the Superdex 200 10/300 GL column was instrumental for the generation of milligram scale preparations of the individual protein components, but it was less suitable for high-resolution analysis of products. The updated Superdex 200 10/300 pg Increase column offered higher resolution; however, other specialized columns may be more appropriate for this study. We hypothesize that a column containing resin with a larger pore size would aid in resolving the higher molecular weight reconstitution products.

Lastly, careful study of the published literature can be extremely helpful in troubleshooting problematic experiments. Specifically, the structural work on protein nanodiscs by Hagn et al. provided important insight into the chromatographic profiles of MSP3 and MSP1 [3]. This study offered an explanation for the formation of large MSP aggregates and provided clear instructions as to how to minimize aggregates in reconstitutions. Additionally, an EPR study on the maltose transporter provided a valuable estimate of the molecular mass of MalFGK$_2$-MSP3 nanodiscs. These results were particularly useful for our studies since the nanodiscs from the EPR study used a similar lipid stock and a highly-related *E.coli* Type I ABC transporter [4].

4.3 Verification of MetNI Nanodisc Formation

In the end, the most definitive evidence of successful MetNI nanodisc formation was obtained through a co-immunoprecipitation method. This protocol, while costly in reagents, was invaluable for our project. Used in combination with native PAGE and SDS-PAGE, the co-immunoprecipitation revealed the formation of a single stable MetNI nanodisc complex.

4.4 Increasing the Yield of MetNI Nanodiscs

The yield of the reconstitution process became a major concern early on in our reconstitution trials. Once we developed appropriate analysis methods, we focused on the optimization of scaled-up conditions. Scaling-up of reactions often do not produce the anticipated results, and thus we explored different molar ratios of components and found that the addition of sodium cholate was critical in minimizing contaminants. As described in detail in the results section, we ultimately determined that a molar ratio of 1:3:60 of MetNI : MSP1 : lipid with 1.5 relative amounts of cholate was the optimal condition for assembly. These conditions were reproducible and generated sufficient amounts of MetNI-ND1 for our preliminary functional studies.

4.5 MetNI-ND1 Does Not Exhibit Decreased Basal Activity

As previously stated, the ultimate goal of this research was to test an alternative membrane system for biochemical studies of the MetNI transporter. Studies in related systems demonstrated that detergent-solubilized transporters may not faithfully reproduce the activity of membrane-embedded transporters [5-7]. Thus, we sought to compare MetNI activity in nanodiscs versus detergents.

In detergent-based assays, MetNI hydrolyzes ATP in the absence of substrate, thereby futilely consuming energy. Our initial hypothesis stated that MetNI in a lipidic environment would not exhibit this wasteful ATP hydrolysis. To test this idea, we measured ATP hydrolysis using a conventional ATPase protocol. The K_M and k_{cat} of ATP hydrolysis was determined using standard kinetic models. Surprisingly, both forms of MetNI demonstrated similar levels of basal futile ATP hydrolysis. The same results were observed for a MetNI variant that is not susceptible to transinhibition. These findings refute our hypothesis and indicate that the lipid environment provided by the nanodiscs does not decrease the basal ATPase activity.

4.6 Proposed Future Work on the MetNI Transporter

While the findings from the functional studies above are somewhat disappointing, this work has highlighted various assumptions and shortcomings in our understanding of methionine transport. For example, we assume that MetNI futile cycling is an artifact of our simplified biochemical system, and that this activity is not present in bona fide membranes or *in vivo.* It is plausible, however, that MetNI in the cell may indeed consume ATP at this rapid pace, or that an additional protein component may play a role in regulating the system. While investigation of these possibilities is beyond the scope of this work, they provide a basis for future study.

Our functional assays using MetNI nanodiscs were preliminary and also warrant further investigation. One important component that is missing from our studies is the substrate binding protein MetQ. The presence of MetQ is a requirement for methionine transport *in vivo*; however, we omitted MetQ from our assays in order to simplify these initial studies. In more recent unpublished studies from the Yang Lab, it was determined that the addition of MetQ stimulates the ATPase activity of detergent-solubilized MetNI beyond basal levels. It will be of great interest to determine how the presence of MetQ alters ATPase activity of MetNI nanodiscs.

4.7 Nanodiscs and Alternative Membrane Systems for ABC Transporter Studies

ABC transporters and alternative membrane environments continue to be topics of interest in biomedical and structural research. The lipid content of a membrane varies significantly based on the cell type, and in the case of eukaryotes, on the type of organelle within a single cell type. In addition, the lipid composition of a certain cell or organelle has been shown to be a critical determinant of *in vivo* function [8].

The effects of lipid composition on ABC transporter function have been studied via non-denaturing tandem native mass spectrometry and functional studies. In a study of McjD, the antibacterial peptide ABC exporter, it was determined that specific lipid types at the TMD-lipid interface are essential to McjD function and stability [9]. In a different study, the mass spectrum of the ABC transporter TmrAB showed a strong preference for defined lipid types. In addition, despite the use of various detergents to solubilize membranes, TmrAB retained its endogenous lipids, suggesting that these lipids bind the TMDs with high affinity [10]. In contrast, studies by the same group showed that some ABC importers do not show a strong preference for certain lipids [11]. Overall, these fascinating observations could be further complemented by functional studies of ABC transporters in nanodiscs of defined lipid composition.

Lastly, a different membrane mimetic has recently been developed for the biochemical study of membrane proteins. Styrene-maleic acid polymeric lipid particles (SMALPs) allow for the isolation of target proteins without the use of detergents. This technology allows for the partial retention of the native lipid environment, unlike nanodiscs and synthetic liposome systems [12]. Future experiments will determine if SMALPS are a tractable alternative for the MetNI transporter.

Overall, the work described in this thesis has laid the groundwork for the study of the MetNI transporter in a lipidic environment. These studies will inform future research on the mechanism of methionine transport in the Yang Lab.

4.8 References

[1] Bao, H.; Duong, F. Discovery of an auto-regulation mechanism for the maltose ABC transporter MalFGK2*. PLoS ONE* **2012,** 7(4): E34836.

[2] Wittig, I.; Schägger, H. Advantages and limitations of clear-native PAGE. *Proteomics* **2005,** 5(17), 4338–4346.

[3] Hagn, F.; Nasr, M. L.; Wagner, G. Assembly of phospholipid nanodiscs of controlled size for structural studies of membrane proteins by NMR. *Nature Protocols* **2018**, 13(1), 79–98.

[4] Alvarez, F. J.; Orelle, C.; Davidson, A. L. Functional reconstitution of an ABC transporter in nanodiscs for use in electron paramagnetic resonance spectroscopy. *Journal of the American Chemical Society* **2010**, 132(28), 9513–9515.

[5] Borch, J.; Hamann, T. The nanodisc: a novel tool for membrane protein studies. *Biological Chemistry* **2009**, 390(8), 805–814.

[6] Bao H.; Dalal K.; Wang V.; Rouiller I.; Duong F. The maltose ABC transporter: action of membrane lipids on the transporter stability, coupling and ATPase activity. *Biochimica et Biophysica Acta* **2013**, 1828, 1723–1730.

[7] Alvarez, F. J.; Orelle, C.; Huang, Y.; Bajaj, R.; Everly, R. M.; Klug, C. S.; Davidson, A. L. Full engagement of liganded maltose-binding protein stabilizes a semi-open ATP-binding cassette dimer in the maltose transporter. *Molecular Microbiology* **2015**, 98(5), 878–894.

[8] Casares, D.; Escribá, P. V.; Rosselló, C. A. Membrane Lipid Composition: Effect on Membrane and Organelle Structure, Function and Compartmentalization and Therapeutic Avenues. *International Journal of Molecular Sciences*, **2019**, 20(9), 2167.

[9] Mehmood, S.; Corradi, V.; Choudhury, H. G.; Hussain, R.; Becker, P.; Axford, D.; Zirah, S.; Rebuffat, S.; Tieleman, D.; Robinson, C.; Beis, K. Structural and Functional Basis for Lipid Synergy on the Activity of the Antibacterial Peptide ABC Transporter McjD. *The Journal of Biological Chemistry* **2016**, 291(41), 21656–21668.

[10] Bechara, C.; Nöll, A.; Morgner, N.; Degiacomi, M.; Tampé, R.; Robinson, C. A subset of annular lipids is linked to the flippase activity of an ABC transporter. *Nature Chemistry*, **2015**, 7(3), 255–262.

[11] Fiorentino, F.; Bolla, J.; Mehmood, S.; Robinson, C. A. The Different Effects of Substrates and Nucleotides on the Complex Formation of ABC Transporters. *Structure* **2019**, 27(4), 651–659.E3.

[12] Postis, V.; Rawson, S.; Mitchell, J.; Lee, S.; Parslow, R.; Dafforn, T.; Baldwin, S.; Muench, S. The use of SMALPs as a novel membrane protein scaffold for structure study by negative stain electron microscopy. *Biochimica et Biophysica Acta* **2015**, 1848(2), 496–501.